Copyright Warning & Restrictions

The copyright law of the United States (Title 17, United States Code) governs the making of photocopies or other reproductions of copyrighted material.

Under certain conditions specified in the law, libraries and archives are authorized to furnish a photocopy or other reproduction. One of these specified conditions is that the photocopy or reproduction is not to be "used for any purpose other than private study, scholarship, or research." If a, user makes a request for, or later uses, a photocopy or reproduction for purposes in excess of "fair use" that user may be liable for copyright infringement,

This institution reserves the right to refuse to accept a copying order if, in its judgment, fulfillment of the order would involve violation of copyright law.

Please Note: The author retains the copyright while the New Jersey Institute of Technology reserves the right to distribute this thesis or dissertation

Printing note: If you do not wish to print this page, then select "Pages from: first page # to: last page #" on the print dialog screen

ABSTRACT

MICROPOROUS SILICON DIOXIDE/VYCOR MEMBRANES FOR GAS SEPARATION

by
Justin R. Barone

This study focused on producing membranes for molecular sieving of gases by reducing the pore size of an already existing membrane structure. To do this, SiO_2 was deposited inside the pores of a Vycor tube with initial pore diameter of 4 nm. The film deposition took place by a low pressure chemical vapor deposition (LPCVD) process where diethylsilane (DES) and nitrous oxide (N_2O) were used as precursor gases. A counterflow reactant geometry was used where the precursor gases were flowed on both sides of the porous membrane. This deposition geometry gave higher selectivities and better mechanical stability. The flows of H_2, He, N_2, Ar, toluene, and dichloromethane (DCM) were monitored in-situ after each deposition. Selectivities on the order of 1000:1 were observed for H_2 and He over N_2. It was also shown that N_2/toluene selectivities of 40:1 were also possible.

MICROPOROUS SILICON DIOXIDE/VYCOR MEMBRANES FOR GAS SEPARATION

by
Justin R. Barone

A Thesis
Submitted to the Faculty of
New Jersey Institute of Technology
in Partial Fulfillment of the Requirements for the Degree of
Master of Science in Engineering Science

Interdisciplinary Program in Materials Science and Engineering

January 1997

APPROVAL PAGE

MICROPOROUS SILICON DIOXIDE/VYCOR MEMBRANES FOR GAS SEPARATION

Justin R. Barone

Dr. Roland A. Levy, Thesis Advisor — Date
Professor of Physics
Director of Materials Science and Engineering Program, NJIT

Dr. Lev N. Krasnoperov — Date
Professor of Chemical Engineering, Chemistry and
Environmental Science, NJIT

Dr. James M. Grow — Date
Professor of Chemical Engineering, Chemistry, and
Environmental Science, NJIT

BIOGRAPHICAL SKETCH

Author: Justin R. Barone

Degree: Master of Science

Date: January 1997

Undergraduate and Graduate Education:

- Master of Science in Engineering Science,
  New Jersey Institute of Technology,
  Newark, New Jersey, 1996

- Bachelor of Science in Materials Science and Engineering,
  Lehigh University,
  Bethlehem, Pa, 1995

Major: Materials Science and Engineering

This thesis is dedicated to
my dear parents

ACKNOWLEDGMENT

The author wishes to express his sincere gratitude to his advisors, Professor Roland A. Levy, Professor Lev. N. Krasnoperov, and Professor James M. Grow for their guidance, encouragement, inspiration, and financial support throughout this research.

The author appreciates the timely help and suggestions from the CVD laboratory members, including: Vitaly Sigal, Jan Opyrchal, Chenna Ravindranath, Kiran Chatty, Vijayalkshmi Venkatesan, Krit Aryusook, Wiriya Thongruang, and Sutham Niyomwas.

TABLE OF CONTENTS

TABLE OF CONTENTS
(Continued)

TABLE OF CONTENTS
(Continued)

LIST OF TABLES

LIST OF FIGURES

CHAPTER 1

INTRODUCTION

1.1 Progress in Ceramic Membrane Technology

Gas separation is important in processes involving oxygen enrichment, inert gas generation, as well as hydrogen, helium, and hydrocarbon recovery[1,2]. It is also a subject of growing interest in studies concerned with the emission reduction of volatile organic compounds (VOC's)[3,4]. Although there are a number of methods, such as adsorption and absorption, to achieve gas separation, the use of membranes offers an attractive alternative because of the associated low capital investment, high processing flexibility, and simple operation. It is in this realm of separation technology that microporous ceramic membranes have gained considerable interest and the improvements in their synthesis have been developing at a rapid pace.

In the past, polymeric membranes[5] were used for separation of mixtures in process industries. On a large scale, these polymeric membranes were utilized in the oxygen enrichment of air, hydrogen separation from carbon monoxide and other gases, removal of carbon dioxide from natural gas, and the reduction of organic vapor concentration in air. Other, smaller scale applications include the preservation of food such as apples and bananas during transport by blanketing with low-oxygen-content air, the generation of inert gases for safety purposes, and the dehydration of gases[6]. Polymeric membranes continue to be

an active area of research, with current emphasis on specialized applications such as ion separation in electrochemical processes, membrane based sensors for gas and ion detection, and membrane reactors. Probably the largest area of active research in polymer membranes is in the biomedical field and the use of membranes in dialysis of blood and urine, artificial lungs and skin, the controlled release of therapeutic drugs, and the affinity separation of biological molecules. The single feature which distinguishes polymers from any other type of membrane material is that they contain a fibrillar structure and great size (macromolecules) which in turn result in cohesive forces which extend to the macroscopic level[7]. Moreover, because of relative ease of processing, the pore sizes and their distribution can be tailored to obtain any desired properties. However, despite their many advantages, polymeric membranes still cannot meat the demands of high temperature applications. One of the main reasons for this is the fact that polymers, being organic compounds[8] with relatively weak bonds, are unstable at high temperatures and soften to such an extent that they collapse under their own weight. It is because of this fact that ceramic membranes have attracted scientific interest.

To most users, ceramic membranes are a relatively new product. In actuality, their use extends over the past half of a century, starting with the development and mass production of membranes for the separation of uranium isotopes by the process of gaseous diffusion applied to UF_6. Fifteen years ago, ceramic membranes were developed for use in the ultrafiltration and

microfiltration of process liquid streams. They have evolved into important tools for beverage production, water purification, and the separation of dairy products[9]. The most recent research involves separations using a variety of basic processes, including the coupling of catalytic reactions and membrane separations. Ten years ago, the ceramic membranes employed for gas separations were typically based on the use of Knudsen diffusion as the primary mechanism of transport. However, currently available ceramic membrane technology allows one to utilize not only Knudsen diffusion but also surface activated transport as vehicles for bringing about molecular separations. Table 1.1 gives a list of some of the currently available inorganic ceramic membranes.

Table 1.1 Commercial ceramic membranes

Manufacturer	Membrane material	Diameter of pores in the membrane
US Filter	ZrO_2	20 nm
US Filter	Al_2O_3	5 nm
Alcan/Anotec	Al_2O_3	20 nm
Gaston County Filtration Systems	ZrO_2	4 nm
Rhone-Poulenc/SFEC	ZrO_2	4 nm
TDK	ZrO_2	~10 nm
Schott Glass	Glass	10 nm
Fuji Filters	Glass	4 nm

However, currently available ceramic membranes possess pore diameters that are no less than 4 nm in size. These are the membranes that are separating gases primarily by Knudsen and surface diffusions, as described above. But, the selectivities achieved are still low. Through a uniform reduction of the pore size in the Vycor substrate down to a nanoscale level (~ 0.5 nm), gas separation can be dramatically enhanced due to the change in the gas transport mechanisms from the mesoporous to the microporous regime. In the mesoporous region where Knudsen diffusion dominates, selectivities are proportional to the inverse square root of the molecular weight ratios of the permeant gases[10-12]. In the microporous range, higher selectivities are achieved primarily as a result of molecular sieving effects[11,13,14].

1.2 Advantages of Ceramic Membranes and Future Technology

Inorganic membranes are more expensive than organic polymeric membranes, but ceramic membranes have the ability of providing extremely high filtration surface area and therefore great economy-of-scale, making them cost-effective[5]. Ceramic membranes are temperature and wear resistant. Ceramic membranes are in fact stable up to about 1000°C[15]. Ceramic membranes are processed by starting with assemblies of crystals and particles. As a result of the compact crystal structure and chemical bonding characteristic of the small and highly charged cations, ceramic membranes have very good structural integrity. This allows them to be used at the very high pressures (~30 atm) associated with

high throughput. This obviously leads to more efficient energy use and economical savings. Porous membranes tend to have a well-defined, stable pore structure and are chemically inert, making them resistant to a wide variety of solvents, acids, alkalines, and detergents. These advantages encouraged researchers in the 1980's to investigate the gas separation properties and applications of ceramic membranes in membrane reactors. At present, the biggest challenge is to transfer the theoretical aspects of the technology to the applied aspects so valuable to industry. Applications being considered include economical, clean processes and energy conversion, new sensors, and separation problems in the fields of environmental technology and water treatment, which is the pertinent application of this study.

1.3 Ceramic Membrane Materials and Applications

Ceramic membranes can be deposited on a support or made as such in the form of a plate of active material[9]. Supported membranes are commonly used at high temperature. Usually, a ceramic film is deposited onto a substrate[16] which has a larger mean pore size. The substrate will typically be the load bearing member of the membrane and therefore must maintain its mechanical integrity over a wide temperature and pressure range. Concurrently, the substrate also must be microcrack and defect free. It must be able to withstand the highly corrosive environment in which it is placed. The substrate has to have a large surface area to allow for high throughput with the mesopores providing all of the inherent

permeability. Finally, these pores should be of a very narrow size distribution. In this study, an additional property, the coefficient of thermal expansion comes into effect. This can be related to structural integrity at high temperatures, but for this application, the difference between the coefficients of thermal expansion for the support and the deposit should be as low as possible to reduce the possibility of microcrack formation in the membranes, the primary source of membrane failures.

The substrate used in our study was a porous Vycor tube manufactured by Corning Inc., and is commercially available as Vycor 7930. Vycor glass is made up of 96% SiO_2, the rest being B_2O_3. Processing of the substrate is discussed in the next chapter.

Typical ceramic materials include alumina, zirconia, titania, silica, carbon, and silicon carbide. These membranes can come in several configurations: hollow fibers, flat plates, honeycombs and hollow tubes.

These types of ceramic membranes find increasing use in the following applications:

- gas separation: involves mainly the removal of hydrogen from refinery stream, and carbon dioxide and hydrogen sulfide from natural gas.
- biotechnology/pharmaceutical: Removal of viruses from culture broth and purification of amino acids, vitamins, and organic acids.
- petrochemical: catalytic dehydrogenation[16] of large molecules at low temperatures and also used for coal gasification.

- environmental control: To get rid of precipitated radionuclides and metaloxides.
- concentration and homogenization of milk and eggs.
- metal refining: removal of impurities and undesirable metal oxides from superalloys.

Innovative applications are still being discovered such as an integrated membrane[18]. This composite membrane consists of a selective layer and a catalytic layer. The selective layer allows the migration of only the reactant and blocks the impurities. The reactant then comes in contact with the catalytic layer where it is converted into the product and is subsequently swept off by convective forces. The benefits of such a process are highly simplified processing, no byproducts, and faster kinetics. A prototype has been developed for use in hydrocarbon oxidation and hydrogenation processes.

1.4 SiO_2 as a Membrane Layer

The reason for selecting SiO_2 as the membrane layer was due to the matched coefficients of thermal expansion between the film and the substrate, which would minimize film cracking during thermal cycling[7]. So films of SiO_2 could be deposited using diethylsilane (DES) and N_2O, diethylsilane being the source for silicon. Silicon dioxide films produced from DES have been shown to exhibit better conformality, lower stress, and higher crack resistance than those produced from SiH_4[20-22]. Aside from silane[23,24], other reported precursors used

in the synthesis of CVD SiO_2 films for membrane applications include $SiCl_4$[25,26] and triisopropylsilane[27]. Oxygen was the most commonly used precursor in the CVD synthesis of SiO_2 films[22-24,27], until the study started by Levy[28] et al where N_2O was first used. In that study, the use of N_2O as a precursor gas was believed to make the process self-limiting. When the pore diameter approaches the size of the N_2O molecule, no further reactions would be expected and film deposition would automatically stop. The selection of N_2O with a diameter less than that of a typical VOC but greater than that of N_2 would block the flow of the larger sized molecules while still permitting N_2 to flow through the membrane. Also, silicon dioxide has some very attractive inherent properties which make it a potential competitor as a membrane material. SiO_2 has low moisture absorption and low compressive stress. The principal physical properties of SiO_2 are given in Table 1.2.

1.5 Use of DES as a Precursor Gas

Extensive work has been done on the chemical vapor deposition of silicon dioxide thin films on various substrates including silicon, quartz, and glass[20-25]. A wide range of precursors have been used as a source for silicon to obtain these thin films including silane[23,24], silicon tetrachloride[25,26], triisopropylsilane[27], and diethylsilane[20-22]. DES is a colorless liquid with a boiling point of 56°C and a freezing point of -76°C. It has a high enough vapor pressure (207 torr at 20°C) for easy delivery and control of the gas in the LPCVD reactor. In fact, DES can

be processed into the reactor without the need of a carrier gas. Heating of the liquid source and the delivery line is not necessary either. Also attractive is the fact that DES is environmentally benign, satisfying any safety or environmental concerns. The properties of DES are given in Table 1.3.

Table 1.2 Properties of silica

Boiling Point(°C)	~2950
Melting Point (°C)	~1700
Molecular Weight	60.08
Refractive Index	1.46
Specific Heat (J/g°C)	1.0
Stress in Film on Si (dyne/cm^3)	2-4 x 10^9, compressive
Thermal Conductivity(W/cm°C)	0.014
DC Resistivity (Ω-cm), 25°C	10^{14}-10^{16}
Density (gm/cm^3)	2.27
Dielectric Constant	3.8-3.9
Dielectric Strength (V/cm)	5-10x10^6
Energy Gap (eV)	~8
Etch rate in Buffered HF (nm/min)	100
Linear Expansion Coefficient (cm/cm°C)	5x10^{-7}

Table 1.3 Properties of DES

Chemical Name	Diethyl silane (DES)
Chemical Formula	$SiH_2(C_2H_5)_2$
Molecular Weight (g/mol)	88.2
Specific Gravity (g/cm^3 @ 20°C)	0.6843
Freezing Point (°C @ 1 atm)	<-76
Boiling Point (°C)	56
Appearance	Colorless liquid
Vapor Pressure (torr @ 20°C)	207
Vapor Density (air = 1)	> 1

CHAPTER 2

TECHNIQUES FOR MEMBRANE SYNTHESIS

Many methods have been used to synthesize ceramic membranes, such as sol-gel, slip-cast, acid-leach, dense membranes, and pyrolysis. Here, an overview is given of each.

2.1 Sol-Gel Technique

The sol-gel process can be divided into two main routes, the colloidal suspension route and the polymeric gel route[29]. In both cases, an inorganic salt or a metal organic precursor is hydrolyzed while simultaneously a condensation or polymerization reaction occurs. It is important that the hydrolysis rate with respect to the polycondensation rate be controlled. In the colloidal route, a faster hydrolysis rate is obtained by reacting the precursor with excess water. A precipitate of hydrated oxide particles is formed which is peptized in a subsequent step to a stable colloidal suspension. The elementary particle size ranges, depending on the system and processing conditions, from 3-15 nm and these particles from loosely bound aggregates with sizes ranging from 5-1000 nm. By increasing the concentration of the suspension and/or by manipulation of the surface potential of the sol particles the colloidal suspension is transformed to a gel structure consisting of interlinked chains of particles or agglomerates.

The hydrolysis and polymerization rate of metal organic compounds can generally be better controlled than those of metal salts. The chemical reaction involves two steps:

1. The partial hydrolysis of the metal organic compound introduces the active functional OH groups, attached to metal atoms.
2. These then react with each other or with other reactants to form a polymeric solution which further polymerizes to form a viscous solution of organic-inorganic polymeric molecules.

In the polymeric gel route, the hydrolysis rate is kept low by adding successively small amounts of water. The final stage of this process is a strongly interlinked gel network with a structure different from that obtained from the colloidal route. This is because the network formation takes place continuously within the liquid. It is not necessary to remove this liquid to obtain a gel as in the colloidal route[30,31].

The size of the particles in the sol strongly determines the size of the final pore and can be tailored by changing the pH of the medium, the molar ratios of metal organics, temperature, feed rate of the reactants etc., The particles have to be uniformly[32] distributed in the medium to obviate any non-uniform deposit. Also, the particles have to behave individually rather than act together as an agglomerate. For this purpose stabilizing or deagglomerating agents such as aliphatic acids, or bases are added to control the pH of the sol and thus inducing surface charge on the particles.

Sol gel technique is extensively used for alumina, zirconia and titania membranes. One of the main limitations of this technique is that the pore size is strongly dependent on the particle size which cannot be obtained accurately. The final pore sizes rarely cross below the 4 nm diameter and hence are useful for ultrafiltration. Research in this field is directed mainly at obtaining finer particles with diameters of approximately 3 nm.

2.2 Slip-Casting

A common method to slip-cast[33] ceramic membranes is to start with the colloidal suspension or the polymeric solution of the sol-gel process described in the previous section. This is known as the slip. A porous substrate is dipped in the slip and a dispersion medium, i.e. water or water-alcohol mixtures, is forced into the pores of the support by a pressure drop created by capillary action of the microporous support[34]. At the interface, the solid particles are retained and concentrated at the entrance of the pores to form a gel layer as in the case of sol-gel processes. It is important that formation of the gel layer starts immediately and that the solid particles do not penetrate the pores of the substrate system. This means that the solid concentration in the slip must not be too low, the slip must be close to its gelling state, and the particle size must not be too small compared with the pore size of the substrate. The smaller and more uniform the primary particles and the weaker the agglomerates in the sol are, the smaller the pore size and the narrower its distribution in the membrane.

The rate of membrane deposition can be increased by increasing slip concentration or decreasing the pore size of the substrate.

The final stage is the firing of the gelled sol along with the support. A thorough understanding of the phase changes and thermal/hydrodynamic stresses developed during firing is essential to hold the membrane to the support.

2.3 Acid Leaching

Turner and Winks[25] first performed acid-leaching in 1926 on glasses containing boric oxide using hydrochloric acid. Glass membranes with an isotropic spongy structure of interconnected pores can be prepared by thermally demixing a homogenous Na_2O-B_2O_3-SiO_2 glass phase into two phases. The alkali-borosilicate glass separates into a phase that is almost pure silica and a phase that is rich in Na_2O and B_2O_3. As the temperature is lowered, a tendency to form Na-O-B bonds rather than Na-O-Si bonds is developed. Simultaneous separation proceeds into an insoluble phase(-Si-O-Si-) and a soluble phase(-Na-O-B-)[26]. The latter phase is then leached by either an acid, base, or just water, thereby creating a porous structure in the SiO_2 phase. The pore size and distribution can be controlled by the concentration of the leachable phase and by carefully monitoring the time and temperature during the thermal decomposition.

Acid leaching is a complicated process and extreme care has to be taken to obtain defect free porous glass. A strain is set up, partly from purely physical

causes, because of capillary forces developing in the pores due to the presence of acid. The strain can be induced either by *swelling* of the leached layer or by *shrinking*. Glass is then scrubbed with water and dried slowly to remove excess water.

When the thermal treatment occurs at temperatures less than 400°C, the rate of redistribution of soluble component is slow and nucleation of the second phase does not occur[35]. Acid leaching at this stage results in a microporous glass with a pore size of 0.5 to 2 nm. However, when the homogenous amorphous phase is thermally treated above 400°C, irreversible nucleation in the second phase begins. If the two-phase material is leached, a mesoporous glass membrane is formed. This is Vycor glass.

Vycor glass has a pore diameter ranging from 2 - 4 nm and a porosity of about 30%. Porous Vycor glass can absorb atmospheric moisture by as much as 25% of its own weight. These glasses are commercially available as Vycor No. 7930, which is the substrate used in this study.

2.4 Dense Membranes

Dense membranes are essentially composite structures[36]. They consist of thin plates of oxides such as stabilized zirconia or bismuth oxides. These membranes are permeable to ionic forms of hydrogen or oxygen and are usually studied in conjunction with reactions like (oxidative) dehydrogenation, partial oxidation, etc. in membrane reactors[34,37]. Their main drawback is their low

permeability. This can be improved by making very thin micrometer or nanometer layers by deposition in a pore system.

2.5 Pyrolysis

Membranes with extremely small pores (< 2.5 nm diameter) can be made by pyrolysis of polymeric precursors or by modification methods. Molecular sieve carbon or silica membranes with pore diameters of 1 nm have been made by controlled pyrolysis of certain thermoset polymers or silicone rubbers, respectively[38]. When these materials are subjected to controlled pyrolytic conditions, volatiles are emitted and the compound collapses into a stable porous structure. Koresh and Sofer[39] have demonstrated the possibility of preparing highly selective carbon microporous membranes using pyrolysis and there has been continued emphasis on synthesizing molecular sieve structures using this approach.

Molecular sieve dimensions can be obtained by modifying the pore system of an already formed membrane structure. Zeolitic membranes can be prepared by reaction of alumina membranes with silica and alkali followed by hydrothermal treatment[36]. Oxides can be precipitated or adsorbed from solutions or by gas phase deposition within the pores of an already existing structure to modify the chemical nature of the membrane or to decrease the effective pore size. To decrease the pore size, a high concentration of the precipitated material in the pore system is required. This is essentially the aim of this study. Here,

chemical vapor deposition (CVD) is employed to effectively reduce the pore size of a mesoporous membrane by deposition oxide in the pores. The aspect of this technology are discussed next.

2.6 Thin-Film Deposition Methods

Thin-film deposition techniques have traditionally been used in the microelectronics industry for microchip coating, wear and corrosion resistance, and thermal protection. Although it is not the case to produce a porous structure in the microelectronics applications, it is feasible to produce a porous structure by carefully controlling process parameters. Thin-film deposition essentially is used to narrow existing large pores (mesoporous) down to a size which is favorable for separation (microporous). Hence, a porous substrate is required which is free of defects such as cracks or pinholes. Compounds or elements are deposited inside the pores thus narrowing down the pore size. Deposition methods can be classified under two groups: Physical Vapor Deposition (PVD) and Chemical Vapor Deposition (CVD).

2.6.1 Physical Vapor Deposition

Physical vapor deposition (PVD) is mainly focused into two categories, evaporation and sputtering. The objective of these deposition techniques is to controllably transfer atoms from a source to a substrate where film formation and growth proceed atomistically, without the need of a chemical reaction.

In evaporation, atoms are removed from the source by thermal means, whereas in sputtering the atoms are dislodged from a solid target by the impact of gaseous ions. The emergence of PVD as a suitable industrial film deposition process was spurred by advances in vacuum-pumping equipment and Joule heating sources. In general, the properties of the film obtained by PVD are governed by the following: evaporation rate of the atoms, vapor pressure of the target materials, deposition geometry, temperature, pressure, and thermal history of the substrate[40].

Traditionally, evaporation was the preferred PVD technique over sputtering. Higher deposition rates, better vacuum (thus cleaner environments for film formation and growth), and versatility in the fact that all classes of materials can apply were some of the reasons for the dominance of evaporation. The microelectronics revolution required the use of alloys with strict stoichiometric limits which had to conformally cover and adhere well to substrate surfaces. This facilitated the need for the sputtering technique and so, as developments were made in radio frequency, bias, and magnetron variants, so were advances made in sputtering. These variants extended the capabilities of sputtering, as did the availability of high purity targets and working gases. The decision to use either technique depends solely on the desired application and has even spurred the development of hybrid techniques[40]. A comparison of the two is given in Table 2.1.

Table 2.1 Evaporation vs. Sputtering

Evaporation	Sputtering
A. Production of Vapor Species	
1. Thermal evaporation mechanism	Ion bombardment and collisional momentum transfer
2. Low kinetic energy of evaporant atoms (@ 1200 K , E = 0.1 eV)	2. High kinetic energy of sputtered atoms (E = 2-30 eV)
3. Evaporation rate ~ 1.3 x 10^{17} atoms/cm^2-sec	3. Sputter rate ~ 3 x 10^{16} atoms/cm^2-sec
4. Directional evaporation according to cosine law	4. Directional sputtering according to cosine law at high sputter rates
5. Fractionation of multicomponent alloys, decomposition, and dissociation of compounds	5. Generally good maintenance of target stoichiometry, but some dissociation of compounds
6. Availability of high evaporation source purities	6. Sputter target of all materials are available; purity varies with material
B. The Gas Phase	
1. Evaporant atoms travel in high or ultrahigh vacuum (~ 10^{-6} - 10^{-10} torr) ambient	1. Sputtered atoms encounter high pressure discharge region (~ 100 mtorr)
2. Thermal velocity of evaporant 10^5 cm/sec	2. Neutral atom velocity ~ 5 x 10^4 cm/sec

3. Mean-free path is larger than evaporant-substrate spacing; evaporant atoms undergo no collisions in vacuum	3. Mean-free path is less than target-substrate spacing; Sputtered atoms undergo many collisions in the discharge

C. The Condensed Film

1. Condensing atoms have relatively low energy	1. Condensing atoms have high energy
2. Low gas incorporation	2. Some gas incorporation
3. Grain size generally larger than for sputtered film	3. Good adhesion to substrate
4. Few grain orientations (textured films)	4. Many grain orientations

Chemical vapor deposition is discussed next. Some factors that distinguish PVD from CVD are:

1. Reliance on solid or molten sources
2. Physical mechanisms (evaporation or collisional impact) by which source atoms enter the gas phase
3. Reduced pressure environment through which the gaseous species are transported

General absence of chemical reactions in the gas phase and at the substrate surface (reactive PVD processes are exceptions).

2.6.2 Chemical Vapor Deposition

Chemical vapor deposition uses chemically reactive vapors to synthesize or deposit a film or coating. This directly falls under the heading of pyrolysis, as well as disproportionation, reduction, and oxidation. Like PVD, this technique is also a valuable tool for the microelectronics industry. A very large variety of materials can be formed by this method, including those for membrane synthesis[41]. Film properties to control during CVD include thickness, composition, purity, crystallinity, and surface/bulk morphology. Fundamental issues in CVD, which relate directly to film properties, include thermodynamics, kinetics, mass transfer, momentum transfer, heat transfer, reactor design, and process control. All of these will be discussed next.

2.6.2.1 Overview of Chemical Vapor Deposition Process: The individual process steps in the CVD technique are outlined as follows[42]:

1. Mass transport in the bulk gas flow region from the reactor inlet to the deposition zone.
2. Gas phase reactions leading to the formation of film precursors and byproducts.
3. Mass transport of film precursors to the growth surface.
4. Adsorption of film precursors on the growth surface.
5. Surface diffusion of film precursors to growth sites.
6. Incorporation of film constituents into the growing film.

7. Desorption of byproducts of the surface reactions.
8. Mass transport of byproducts in the bulk gas flow region away from the deposition zone towards the reactor exit.

Schematically, this is seen in Figure 2.1.

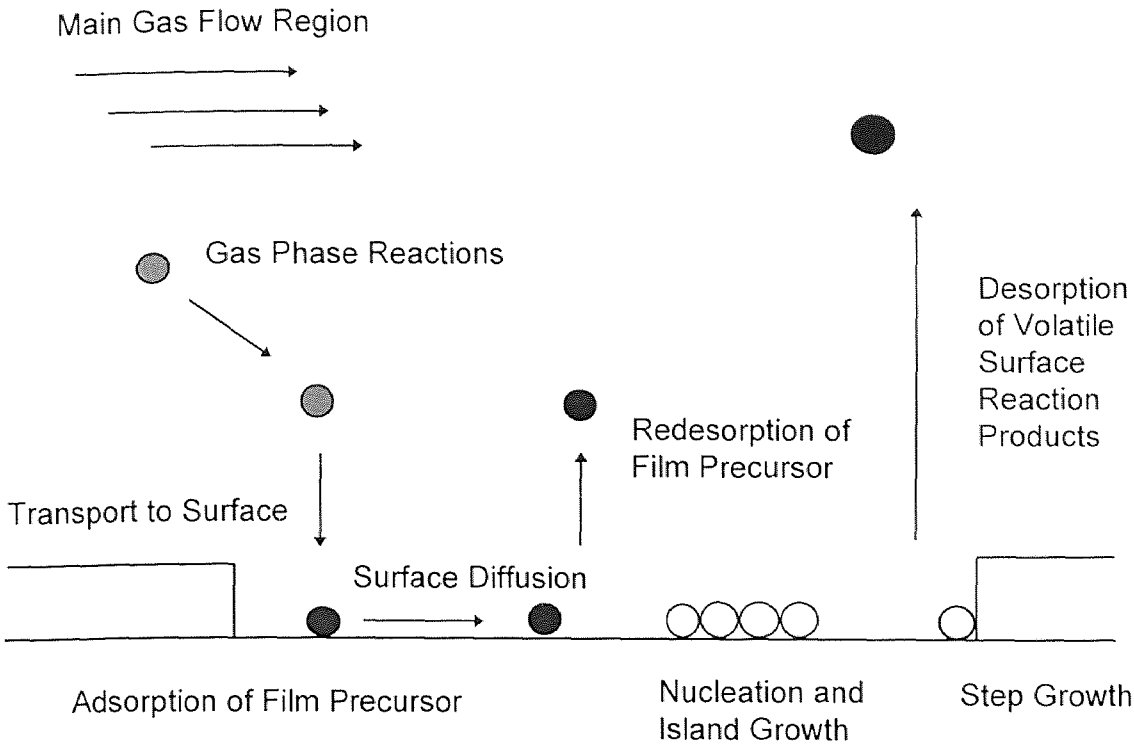

Figure 2.1: Scheme to show the transport and reaction processes underlying CVD.

2.6.2.2 CVD Reactor Systems: CVD reactors are designed to obtain optimal film thickness, crystal structure, surface morphology, and interface composition. A CVD reactor system typically consists of a reagent handling arrangement for delivering the source compounds, a reactor unit, and an exhaust system. The reagent handling system mixes and meters the gas mixture to be used in the

reactor. The design depends on the source compounds. Gaseous sources are fed from a high pressure gas cylinder through a mass flow controller, in this case nitrous oxide. Liquid and solid sources are typically used by contacting them with a carrier gas in a bubbler. The amount of reagent transported from the bubbler is determined by the source temperature, carrier gas flow rate, and the total pressure of the source. In this study, a carrier gas is not needed because of the high vapor pressure of DES and the low pressure nature of the deposition. The need for films with reproducible and controllable optical, electrical, and mechanical properties means that CVD reagents must be pure, must not produce byproducts that incorporate into the growing film or interact with gas handling and reactor construction materials.

There are a wide variety of CVD reactor geometries used to accommodate the many CVD applications. These include horizontal reactor, vertical reactor, barrel reactor, pancake reactor, and multiple-wafer-in-tube LPCVD reactor. Essentially, this study involves a multiple-wafer-in-tube LPCVD (low pressure chemical vapor deposition) reactor modified to accommodate the membrane substrate (instead of wafers). LPCVD is the main production tool for polycrystalline silicon films, especially for the films used in the microelectronics industry[43-45]. A typical configuration for this reactor is shown in Figure 2.2. This reactor operates around 0.5 torr and wall temperatures are approximately equal to those of the deposition surfaces. The main advantage of LPCVD is that is allows a large number of substrates to be coated simultaneously while

maintaining film uniformity. This is a result of the large diffusion coefficient at low pressures, which makes the growth rate limited by the rate of surface reactions rather than the rate of mass transfer to the substrate.

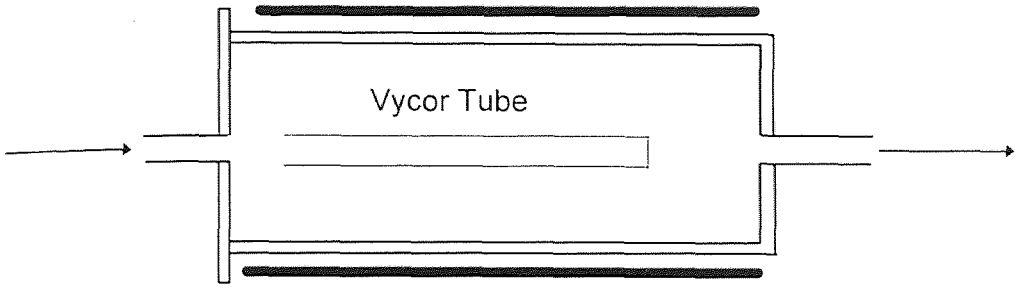

Figure 2.2: LPCVD Reactor.

Finally, the exhaust system treats the effluents so that hazardous byproducts are disposed of in a safe and environmentally sound manner. Mechanical pumps are typically added for the low pressure operation. Dry and wet chemical scrubbers, as well as pyrolysis units, are used to clean up the reactor effluent.

2.6.2.3 Nucleation and Growth: The growth of a thin film by CVD is initiated by exposing a substrate to the film precursors in the reactor. The resulting growth and microstructure of the film is determined by surface diffusion and nucleation processes on the growth interface, which are influenced by the substrate temperature, reactor pressure, and gas-phase composition. An amorphous film

is formed at low temperatures and high growth rates when the surface diffusion is slow relative to the arrival of film precursors. At high temperatures and low growth rates, the surface diffusion is fast relative to the incoming flux, allowing the adsorbed species to diffuse to step growth and to form epitaxial layers replicating the substrate lattice. Nucleation occurs at many different points on the surface at intermediate temperatures and growth rates. Adsorbed species then diffuse to the islands which grow and coalesce to form a polycrystalline film. The presence of impurities increases the nucleation density. CVD film growth modes may be characterized in terms of three main growth models for thin films: Volmer-Weber growth (three-dimensional island growth), Franck-van der Merwe growth (two-dimensional layer by layer), and Stranski-Krastanov growth (layer plus island)[42].

2.6.2.4 Chemical Reactions and Kinetics: The versatility of the CVD technique is demonstrated through the multitude of films synthesized by various reaction schemes, including pyrolysis, reduction, oxidation, and disproportionation of the reactants. The underlying chemistry is typically a complex mixture of gas-phase and surface reactions. The fundamental reaction pathways and kinetics have been investigated for only a few well characterized, industrially important systems. These include silane chemistry (pertinent to this study and discussed in detail in the experimental procedure) and thus silicon deposition, free-radical reactions, and intramolecular reactions of organometallic compounds.

2.6.2.5 Transport Phenomena: Fluid flow, heat transfer, and mass transfer are all characterized under transport phenomena. Transport phenomena govern the access of film precursors to the substrate and influence the degree of desirable and unwanted gas-phase reactions taking place before deposition. The complex reactor geometries and large thermal gradients of CVD reactors lead to a wide variety of flow structures impacting film thickness and composition uniformity, as well as impurity levels. Direct observation of flow is difficult because of a lack of a suitable visualization technique for many systems and because of practical constraints such as no optical access and possible contamination of a production reactor. Therefore, experimental observations and approximately chosen computer models are employed on individual systems[46,47].

CHAPTER 3

MEMBRANE CHARACTERIZATION AND GAS SEPARATION MECHANISMS

The separation efficiency, i.e. permselectivity and permeability, of ceramic membranes depends on microstructural features such as pore size and pore distribution, pore shape, and porosity. Also included in the microstructural characteristics of the membrane is its stability and structural integrity. Several techniques are available to characterize ceramic membranes. These are discussed as are gas separation mechanisms in ceramic membranes. The pore size of the membrane directly affects the transport mechanism through the pores.

3.1 Pore Characterization

Pore size plays an important role in determining permeability and selectivity of a membrane. The structural stability of porous ceramic membranes under high pressures makes them amenable to conventional pore size analysis such as mercury porosimetry and nitrogen adsorption/desorption. Newer techniques which employ nuclear magnetic resonance technology and a method known as permporometry are also used[48,49].

3.1.1 Mercury Porosimetry

Mercury porosimeters can usually provide pore diameter data in the pore range of 3.5 - 7500 nm. The method is useful and very common in the characterization of membranes[50-52]. Mercury is non-wetting on most surfaces and has to be forced into the pore under pressure. The relation between the pore size, r, and the applied pressure, P, is given by

$$r = \frac{-2\gamma \cos\theta}{P} \tag{3.1}$$

where γ is the surface energy and θ is the contact angle between the pore walls and mercury. Typical mercury porosimetry data come in two forms, intrusion and extrusion. The intrusion data are more often used because the intrusion step precedes the extrusion step in the mercury porosimetry analysis and the complete extrusion of mercury out of the pores during the depressurization step of the analysis may take a very long time.

3.1.2 Nitrogen Adsorption/Desorption

This works well where mercury porosimetry does not, when the pore size is smaller than 3.5 nm. In fact, it works well for pore sizes between 1.5 and 100 nm. This method is based on the widely used BET theory[48]. The BET theory modifies Langmuir's work relating the volume of a gas adsorbed or desorbed to

the relative pressure, p/p_o. Langmuir assumed a monolayer adsorption/desorption, while Brunauer, Emmett, and Teller account for multilayer adsorption/desorption. Typical data from this method are split into two portions: adsorption and desorption. The nitrogen desorption curve is usually used to describe the pore size distribution and corresponds better to the mercury intrusion curve.

3.1.3 Nuclear Magnetic Resonance

This method employs NMR spin-lattice relaxation measurements to characterize a wide range of pore sizes (<1 to >10000 nm)[53]. Here, the moisture content of the membrane is controlled so that the fine pores in the membrane film are saturated with water, but only a small amount of adsorbed water is in the large pores of the structure. It is known that the spin-lattice relaxation decay of water in a pore is shorter than that for water in the bulk. The relaxation time is the time required for a magnetization of nuclei to reach equilibrium along the magnetic field. From the relaxation times the pore volume distribution can be calculated[54].

$$\frac{1}{t} = \alpha + \frac{\beta}{r} \qquad (3.2)$$

where t is relaxation time, r is pore size, and α and β are constants. It has advantages over the other pore characterization techniques in that it not only

provides data over a larger range of pore sizes, but much larger membrane samples (~ 10 cm) can be used. The size of the sample is only limited by the homogeneity of the magnetic field.

3.1.4 Permporometry

This is a flow-weighted pore size distribution test method based on gas transport rather than volume. It is best suited to gas separation applications because it is not sensitive to the amount of gas adsorbed. In this technique, a mixture of an inert gas and a condensable gas is flowed through membrane pores of various sizes and the flow measured. The gas mixture is pressurized to block the pores by capillary condensation. The pressure is then decreased incrementally and the flow measured first in the large pores, then in the smaller ones. The pressure is decreased until there is no longer an increase in gas flow rate. The flow is measured at each pressure[55]. The change in flow rate between pressures is then related to the pore size by the Kelvin equation for capillary condensation

$$\frac{2\cos\theta}{r} = -\frac{RT}{\sigma V}\ln\left(\frac{p}{p_o}\right) \qquad (3.3)$$

where θ is contact angle between the liquid and the pore wall, V is the molar volume, r is the pore radius, R is the gas constant, T is temperature in Kelvin,

and σ is the kinetic diameter of the diffusant. The test is normally done for small pressure differences across the membrane (< 3 cm Hg) and a low mole fraction (0.05 - 1) of condensable gas. The time required to do the analysis is dictated by temperature and pressure equilibrium times and is typically several hours. It can accommodate membranes of various sizes and shapes[56-58].

3.2 Characterization of the Structural Integrity of the Membrane

A method commonly termed the bubble point test is used to determine if there are any cracks or pinholes in the membrane. It is also found as ASTM F316[59] test procedure. This method relies on the Washburn equation

$$d = 4S\frac{\cos\theta}{\Delta P} \tag{3.4}$$

where d is the pore diameter, S the surface tension of the liquid, θ the contact angle between the membrane and the liquid, and ΔP the applied pressure difference. It is seen that a pressure difference is required to displace a liquid from a pore with a gas such as air or nitrogen. The liquid medium is typically water. A schematic of a typical apparatus to do this type of measurement is given in Figure 3.1. This test is most often used for detecting the largest pore size of the membrane by finding the pressure difference and thus the pore diameter at the first appearance of bubbles from the liquid-saturated membrane

when the test gas pushes the liquid out of the largest size pores. If there are any cracks or pinholes in the structure, the method will notice them as the largest pores and the first bubbles will appear at a much lower pressure than usual.

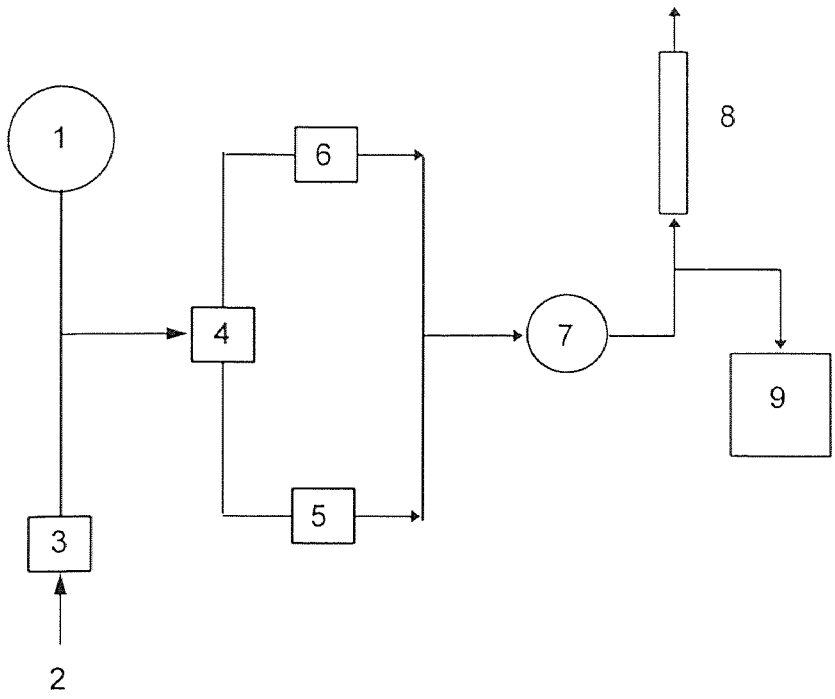

1. Pressure Gauge
2. Pressure Source
3. Pressure Regulator
4. Two-Position Valve
5. Dry Membrane Holder
6. Wet Membrane Holder
7. Liquid Trap
8. Rotameter
9. Bubble Point Detector

Figure 3.1: Schematic of bubble point test apparatus.

3.3 Gas Separation Mechanisms and Transport Phenomena

There are many possible transport mechanisms in a gaseous system. Laminar and turbulent flows, which occur in large pores, and bulk diffusion cannot be used to separate gases. Therefore, useful transport mechanisms for gas separations in porous membranes mainly rely on the following mechanisms, or some combination thereof:

- Knudsen diffusion
- surface diffusion
- capillary condensation
- size exclusion or molecular sieving.

3.3.1 Gas Separation by Knudsen Diffusion

Knudsen diffusion is generally evident when the pore diameter is 5 to 10 nm under pressure or 5 to 50 nm in the absence of pressure. The separation factor is limited by the square root of the molecular weight ratios of the gases being separated. Therefore, it is only practical for the separation of light gases from heavy ones. Several phenomena happen in a typical gas transport[61]. One is molecular diffusion which are molecule-molecule interactions taking place with conservation of total amount of momentum. Next comes laminar flow or viscous flow which is due to molecule-wall interactions. In this collision, the molecule loses momentum to the wall. If there is enough interaction between rebounded and adjacent molecules, the momentum loss is progressively transferred to the

bulk of the gas. Here, there is no segregation of species (as mentioned earlier) and there is a loss of momentum. Finally there is Knudsen diffusion[60]. This is again due to a molecule-wall collision, but this time there is no interaction between a rebounded and adjacent molecule. Therefore, the molecules statistically collide more with the wall than with each other. There are as many gas fluxes as there are species and they are independent of one another, unlike molecular diffusion. Under pressure though, only laminar flow and Knudsen diffusion are relevant. Statistically, if the molecules collide with each other more than the wall of the membrane, the mean free path of the molecules is much smaller than the pore radius, laminar flow dominates over molecular diffusion. If the molecules collide with the membrane wall more than with each other, only Knudsen diffusion occurs[62]. The Knudsen number gives an indication of which type of flow is dominant

$$Kn = \frac{\lambda}{r} \tag{3.5}$$

where λ, the mean free path, is

$$\lambda = \frac{16\eta}{5\pi P_m}\sqrt{\frac{\pi RT}{2M}} \tag{3.6}$$

r is the pore radius, η the gas viscosity, P_m the mean pressure, R the gas constant, T the temperature, and M the molecular mass. Knudsen diffusion occurs for Kn > 1 and is given by

$$F_{o,Kn} = \frac{2}{3}\frac{\varepsilon \mu_k v r}{RTL} \tag{3.7}$$

where v is the mean molecular velocity and is given by

$$v = \sqrt{\frac{8RT}{\pi M}} \tag{3.8}$$

$F_{o,Kn}$ is permeability, ε the porosity, μ_k a shape factor, and L the thickness of the porous medium. Gas separation by Knudsen diffusion can be determined from the ratio of permeability of two gases, A and B

$$\frac{F_{o,A}}{F_{o,B}} = \sqrt{\frac{M_B}{M_A}} \tag{3.9}$$

thus separating gases according to their molecular mass.

3.3.2 Gas Separation by Surface Diffusion

Surface diffusion can be used if the gases to be separated are closer in molecular weight. Here, one component is preferentially absorbed. As it accumulates on the pore surface, the adsorbed component diffuses faster than the other nonadsorbed component. This surface adsorption and diffusion creates a difference in permeability and therefore in separation. It generally works well when the pore diameter is 1 to 10 nm or the surface area is very large[63].

Basically, gas molecules can interact with the surface, adsorb on the surface and move along it. If a pressure gradient is present, a difference in surface occupation occurs. The surface composition gradient created allows transport to occur. The gradient in surface diffusion is known as a surface concentration gradient. The concentration of adsorbed phase is a function of pressure, temperature, and the surface itself. But, the more molecules adsorbed on the membrane, the less the likelihood they will diffuse along its surface. So, controlling the amount of gas adsorbed by the membrane is critical to optimum transport.

Another way to increase the surface diffusion is through a pore size decrease. To describe the relation between surface permeability and the structure of the porous medium for cylindrical pores, the following is used

$$F_{o,s} \sim \frac{\mu_s \varepsilon}{r} \tag{3.10}$$

So, decreasing the pore size increases the surface area of the membrane, and surface diffusion is facilitated. Several models describing surface transport are found in the literature[12,63].

3.3.3 Gas Separation by Capillary Condensation

At low temperatures, some gases will undergo capillary condensation where they occupy the pores of a membrane as a liquid[63,64]. When other gases do not dissolve in the condensed component, separation occurs. Even though this mechanism has been widely used in separation processes involving porous adsorbents, very little is reported in the literature about the dynamic behavior of capillary condensation through porous membranes[34]. This is the pertinent application if separation is desired. Some studies that do not correlate well with each other do exist however[63].

3.3.4 Gas Separation by Molecular Sieving

Molecular sieves are porous media with pores of molecular dimensions. Selectivity is due to the size of the gas molecule. A gas with a kinetic diameter less than the pore will go through while one with a larger kinetic diameter will not. Traditionally, molecular sieves were zeolites or carbon solids[39,63]. Although

much more information is needed in the way of mechanisms that affect molecular sieving (such is the purpose of this study), Koresh and Sofer have come up with a simplistic model describing the separation of a CH_4/H_2 mixture, Figure 3.2. It is assumed that the H_2 and CH_4 molecules reside at different minimum energy positions prior to an activated jump through a pore. The larger molecule will reside at a greater distance than the smaller molecule because of the amorphous character of the membrane.

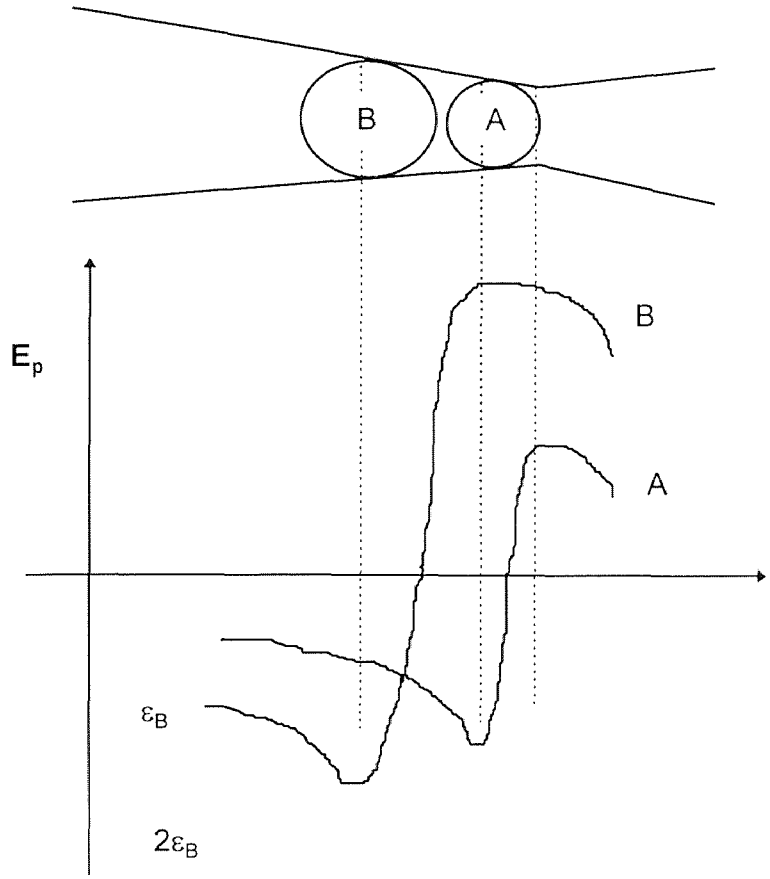

Figure 3.2: The potential energy (E_p) along the permeation path of two molecules of different sizes representing hydrogen and methane.

CHAPTER 4

EXPERIMENTAL PROCEDURE

4.1 Overview of the LPCVD System

The membranes in this study were synthesized in an LPCVD system as shown in Figure 4.1.

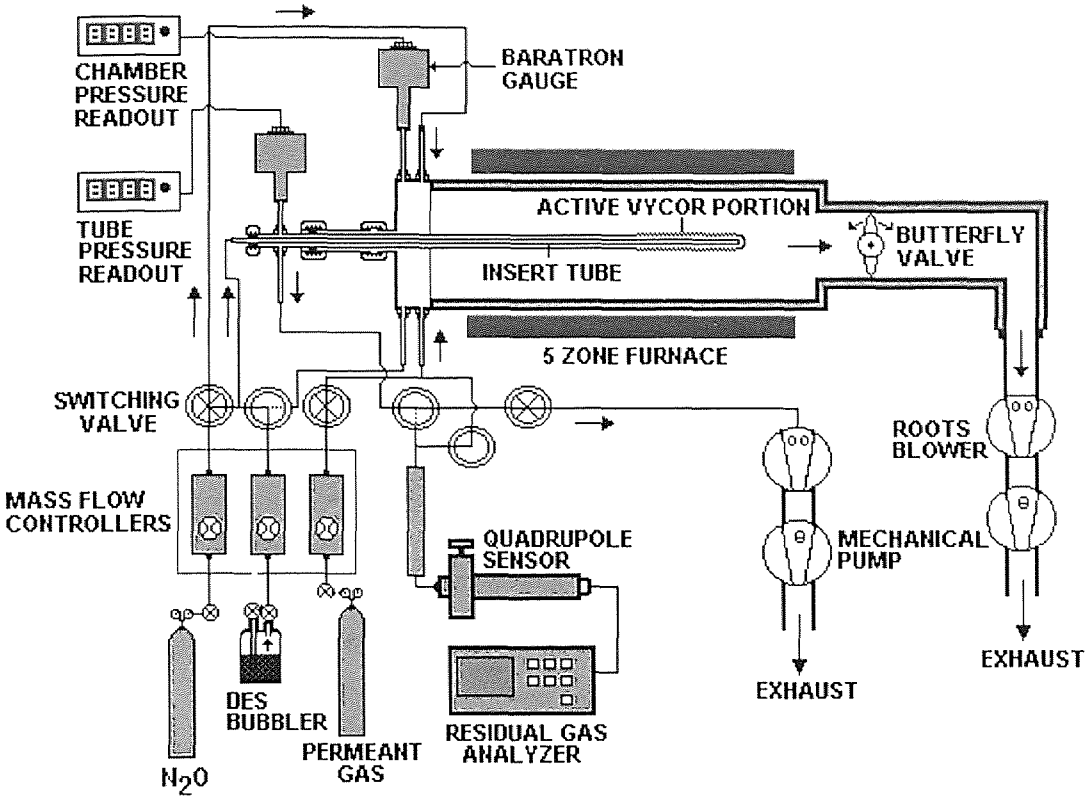

Figure 4.1: LPCVD system for the synthesis of SiO_2 films on Vycor tube.

The reactor was a horizontal fused quartz silica tube having an inner diameter of 19.3 cm and a length of 155 cm. The tube was heated by a five-zone Lindberg furnace providing a uniform temperature distribution across the reactor, heat transfer taking place by convection. This temperature distribution was measured with an Omega type K thermocouple. In this study, only the three middle heating zones of the furnace were used. The two heating zones at the ends were kept closed and high speed fans turned on them to keep them cool and thus protect the delicate Viton O-ring gaskets sealing the quartz tube. The back end of the reactor was connected to an Edwards vacuum system which consisted of a mechanical pump, Model E2M80, and a Roots blower, Model EH500. The other end of the reactor had a door for access to the quartz tube as well as a fixture for inserting the Vycor tube. The reactor pressure was monitored by a standard MKS baratron gauge and the exhaust controlled through the use of an MKS exhaust valve. Also, the reactor had an effective temperature control range up to 1200°C. However, the maximum temperature reached in this study was 450°C. This care was taken to prevent any undesirable sintering of the porous Vycor tube into a non-porous tube.

The precursor gases were DES and N_2O. DES was delivered from a temperature controlled liquid source bottle. Due to the high vapor pressure of DES a carrier gas was not required. Nitrous oxide was delivered from a high pressure gas cylinder. Both precursor gases, as well as the permeant gases, were monitored by using calibrated automatic mass flow controllers, Applied

Materials model AFC 550. Stainless steel delivery lines were used to bring reactants and the permeate gases into the reactor.

4.2 SiO_2/Vycor Membrane Fabrication

4.2.1 Predeposition Procedure

The support structure for the membranes was a porous borosilicate glass tube known as Corning Vycor Glass #7930 with a composition of 96% SiO_2 and 3% B_2O_3. The Vycor glass had an average pore diameter of 40 A and 28% porosity. The tube had an outside diameter of 0.8 cm and a 0.11 cm wall thickness. The tubes were cut into sections and both ends of these sections slowly heated to 1200°C to flow the glass and thus close the pores. This left an active length of 17 cm. One end of the active Vycor tube length was sealed while the other was attached to a similar diameter fused silica tube. This fused silica tube held the membrane in the center of the reactor and allowed for sufficient plumbing of the reactant gases and vacuum lines.

Once prepared, this Vycor tube support structure was inserted into the system through the fixture attached to the front end of the reactor. The LPCVD chamber was evacuated and the temperature slowly raised and kept periodically constant for 15 minutes after 50°C increments until the desired deposition temperature of 450°C was reached. The entire system was pumped down overnight to ensure that all moisture adsorbed by the Vycor tube was eliminated and outgassing from the chamber walls was minimal. After the chamber and

Vycor tube were sufficiently evacuated, the outgassing rate was checked by closing off all valves to the chamber and observing the pressure rise in the reactor. Typical outgassing rates were on the order of ~ 4 mtorr/min.

4.2.2 SiO_2 Deposition

A counterflow geometry to initiate SiO_2 deposition was used. Levy[28] et al showed that the counterflow geometry provided membranes with better stability and selectivity. The counterflow geometry gave an optimum pore narrowing rate inside the pores of the substrate and eliminated the possibility of film cracking. Here, a long, narrow stainless steel tube was inserted inside the Vycor tube, approximately 2 cm from the closed end. First, DES was constantly flowed throughout the deposition from inside the tube at a flow rate of 30 sccm. The vacuum was kept open in the tube to maintain a pressure of DES inside the Vycor of 4 torr. After a stable flow of DES was reached, N_2O was flowed on the outer surface of the Vycor tube at 200 sccm with a pumping rate sufficient to maintain 4.4 torr. N_2O has been shown to give better permselectivity results over other oxidants[28] by providing an enhanced pore narrowing rate. The idea that SiO_2 formation within pores is a self-limiting process also facilitated the use of N_2O as a precursor gas. Here, it was believed that at the point where the pore diameter approaches the size of the N_2O molecule, no further reactions would be expected and film deposition would automatically cease. The selection of N_2O with a diameter less than that of a typical VOC but greater than that of N_2 would

block the flow of the larger sized molecules while still permitting the N_2 to flow through the membrane structure. This may not be the case, however. At the end of deposition, the reactants were turned off and the system allowed to pumpdown overnight so that it was sufficiently evacuated for permeability measurements. When the Vycor tube was finally pumped down to a pressure of ~ 20 mtorr, the membrane was ready for in-situ permeability and selectivity measurements.

4.3 Permeability and Selectivity Measurements

Permeability measurements were done in-situ on the virgin Vycor tube (before deposition) and after each successive deposition. Selectivities were calculated from the permeability data. Typically, a pressure differential was established by introducing one of the permeant gases (H_2, He, Ar, N_2, toluene, or dichloromethane) at a known pressure into the volume outside the Vycor tube and monitoring the pressure increase inside the tube (which was at a very low pressure) with respect to time. Long permeation times were required to render adsorption effects insignificant. Pumping out the reactor chamber overnight to properly evacuate the system after depositions and permeability measurements was also important in keeping adsorption effects to a minimum. The rate of increase of pressure dP/dt inside the Vycor tube was then plotted against the pressure difference created across the membrane. The slope of this plot was converted to permeability coefficients (mol/cm*min*atm) for each of the permeant

gases. This calculation was done based on the known dimensions of each membrane, the volume of the permeate chamber, and the temperature during the measurement. Selectivities were obtained from permeability ratios. These results were confirmed by using on-line mass spectroscopy. The main drawback to this approach was that it only considers the effect of the individual gas on the membrane, whereas interactions due to gas mixtures can behave much differently. This will be shown in the discussion.

CHAPTER 5

RESULTS AND DISCUSSION

The purpose of this study was to test the reproducibility of the results obtained by Levy[28] et al where nitrogen to toluene and argon to toluene selectivities of twenty times the Knudsen value were obtained.

5.1 Virgin Vycor Tube Measurements

Permeability measurements were carried out on a virgin Vycor tube prior to SiO_2 deposition. Figure 5.1 shows that the permeability values are linearly related to the inverse square root of the molecular weight of the gases. This is indicative of Knudsen diffusion and is the result of the mesoporous nature of the virgin Vycor membrane, with pore diameter of approximately 4 nm.

5.2 Deposition of SiO_2 at 450°C

The membranes in this study were produced using the same deposition and test parameters. In some selected depositions however, the flow of DES was reduced to account for an extremely high pressure fluctuation in the Vycor tube. This may have affected the overall properties of the membrane, for example, film thickness, pore diameter, and film stability. All of the films on the membranes were produced using a counterflow reactant geometry with DES flowing inside the tube and N_2O flowing on the outside. This allows the permeabilities of the

test gases to continuously decrease with deposition time and to effectively prevent crack formation[28]. Prior results[28] as well as the results of this study show that high selectivities for H_2 and He relative to N_2 and Ar can be achieved because of the large size differences between these molecules.

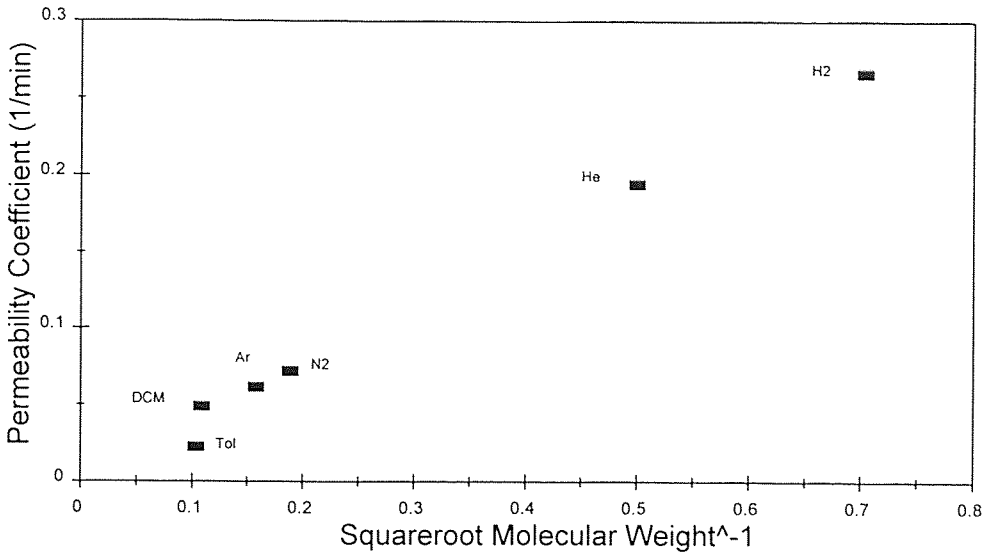

Figure 5.1 Permeability values for virgin Vycor tube.

But, of more industrial relevance is the separation of inerts from volatile organic compounds (VOC's) such as toluene and dichloromethane. In order to achieve good selectivity between species of comparable size such as N_2 and toluene while retaining a high permeability for N_2, the membrane structure should have a narrow pore size range with a final pore diameter that is larger than N_2 (kinetic diameter = 0.374 nm) but smaller than toluene (kinetic diameter = 0.592 nm). To

do this, N_2O is used as a precursor gas. The idea being that SiO_2 film formation within the pores is a self-limiting process. As this study will show, this may not always be the case. Other effects may combine to clog the pore.

5.2.1 Membrane I

This membrane was produced by doing successive depositions with the DES flow rate at 30 sccm and an N_2O flow rate of 200 sccm. This caused a steady pressure of 4 torr inside the Vycor tube for the DES while the N_2O remained at a constant 4.4 torr outside the tube. Figure 5.2 shows the related permeabilities for the test gases permeated through Membrane I. The permeabilities of H_2 and He exhibit an insignificant drop over the entire deposition period of 3.5 hours. This occurred for all membranes and indicated that the Vycor modification was not having a significant effect on their permeabilities. However, the permeabilities of N_2 and Ar dropped by two orders of magnitude. The toluene permeability was so low that it exhibited no linear regression in the dP/dt vs. Pressure Difference curve and can be considered to flow insignificantly through the membrane. Figure 5.3 depicts the selectivities for Membrane I. Due to the low permeation of N_2, Ar, and toluene through the membrane, selectivities were fairly high, with N_2/toluene achieving a selectivity of 27 and Ar/toluene one of 32. These selectivity values were desired, there was good separation between species of similar kinetic diameter. However, these selectivity values came at the cost of inert permeability through the membrane, which is not desired.

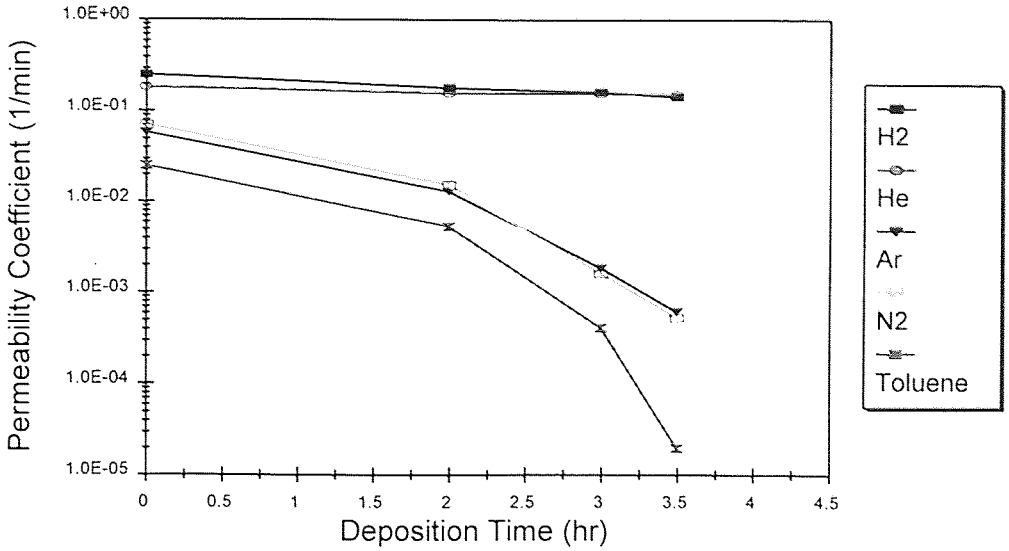

Figure 5.2: Permeabilities for Membrane I.

These results were consistent with those obtained by Levy[28] et al. To confirm them, on-line mass spectroscopy was employed. This proved that there was nitrogen to toluene selectivity. First, permeant gas was introduced into the chamber and allowed to pass through the membrane with time, just like a normal permeability measurement. But, at the end of each permeation done at the respective input pressure (i.e. 5, 10, 13.5 torr) a sample of the gas that has passed through the membrane was taken to be analyzed by the mass spectrometer. No toluene peak was observed when toluene was done by itself while significant nitrogen peaks were observed, confirming flow of N_2 through the membrane. When allowed to scan for increased periods of time (5 to 6 minutes),

the mass spectrometer detected trace amounts of toluene, insignificant compared to the amount of nitrogen detected.

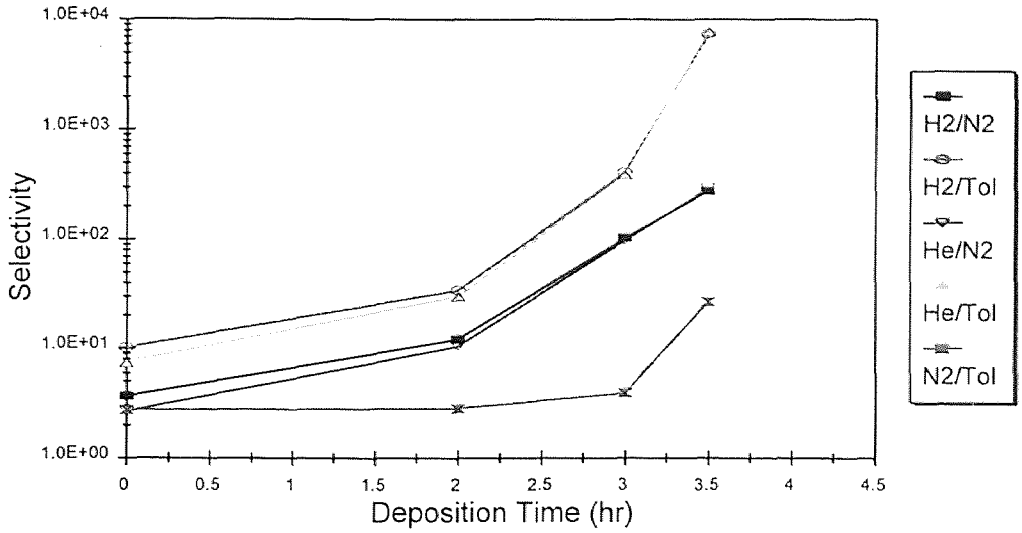

Figure 5.3: Selectivities for Membrane I.

Obviously, adsorption of toluene onto the mass spectrometer was occurring giving increased diffusion times of the sample gas down the collector tube. This prompted the use of a heater on the mass spectrometer that would keep the gas collector tube at 80°C. This decreased the scanning time required to detect toluene to about 4 minutes but still got toluene amounts several orders of magnitude lower than nitrogen.

Now a one-to-one mixture of nitrogen to toluene was permeated through the membrane. The first mass spectrometer measurements showed no toluene

peak appearing at input pressures of 10 torr (5 torr N_2 and 5 torr toluene) and 20 torr (10 torr N_2 and 10 torr toluene). But an input pressure of 28 torr (14 torr N_2 and 14 torr toluene) produced a small toluene peak. It is also noted that the presence of nitrogen in the mixture may be hindering the diffusion of toluene into the mass spectrometer. Again, the heater on the mass spectrometer was set to 80°C and the permeability of the gas mixture analyzed. There was no toluene detected at an input of 10 torr, while at 20 torr there was toluene in the amount of about 1% of the nitrogen concentration, and at an input of 28 torr, toluene was observed to be about 10% of nitrogen. This showed the pressure, time, and temperature dependence of the permeant gas, getting increased permeabilities with increasing pressure, time, and temperature. As more permeability measurements were done on Membrane I, increased amounts of toluene were detected. This indicated the membrane, or more precisely the film, had cracked due to the high temperature (450°C) and repeated pressure differentials induced onto the membrane.

5.2.2 Membrane II

Again, this film was deposited under the conditions described above. However, prior to the first hour of deposition, the DES delivery system was opened too fast, causing a severe pressure rise and the tube to become saturated with DES. The tube was pumped out overnight to ensure that all of the DES was evacuated. During the first hour of deposition, the DES pressure remained at a steady 4.4

torr despite the 30 sccm flow rate. N_2O flow was fine. During the second hour of deposition, both flows were consistent (30 sccm for DES at 4 torr, 200 sccm for N_2O at 4.4 torr). Permeability values consistent with previous membranes were observed over the first two hours of deposition until the central processing unit controlling the reactor failed. This caused a sudden temperature and pressure fluctuation on the tube as the tube began to cool to room temperature and the vacuum was broken, bringing the system quickly to atmospheric pressure. The tube was then removed. Of special note here is the presence of a white deposit in the tube also observed by Levy[28] et al due to gas phase nucleation. The white powdery deposit was observed to be a significant amount most likely because of the initial DES saturation and subsequent pressure fluctuation.

5.2.3 Membrane III

The deposition conditions again remain the same. But, over the entire first hour of deposition, the pressure of DES inside the Vycor tube was observed to fluctuate significantly between 4 and 4.7 torr. However, this was not observed for DES for the other 1.5 hours of deposition. N_2O pressure outside the Vycor tube remained steady at 4.5 torr throughout.

The permeabilities for Membrane III are shown in Figure 5.4. Again, H_2 and He permeabilities remained relatively constant while the permeabilities of the other gases dropped (N_2 by a factor of ~ 7, Ar by a factor of ~ 4, and DCM by a factor of ~ 9), that of toluene dropping by about 2 orders of magnitude (a factor

of ~ 100). Again this lead to good selectivities, as depicted in Figure 5.5. For Membrane III the deposition time was 2.5 hours yielding a N_2/toluene selectivity of 45 and an Ar/toluene selectivity of 63. Membrane I, even after 3.5 hours of deposition, did not yield as good results as Membrane III.

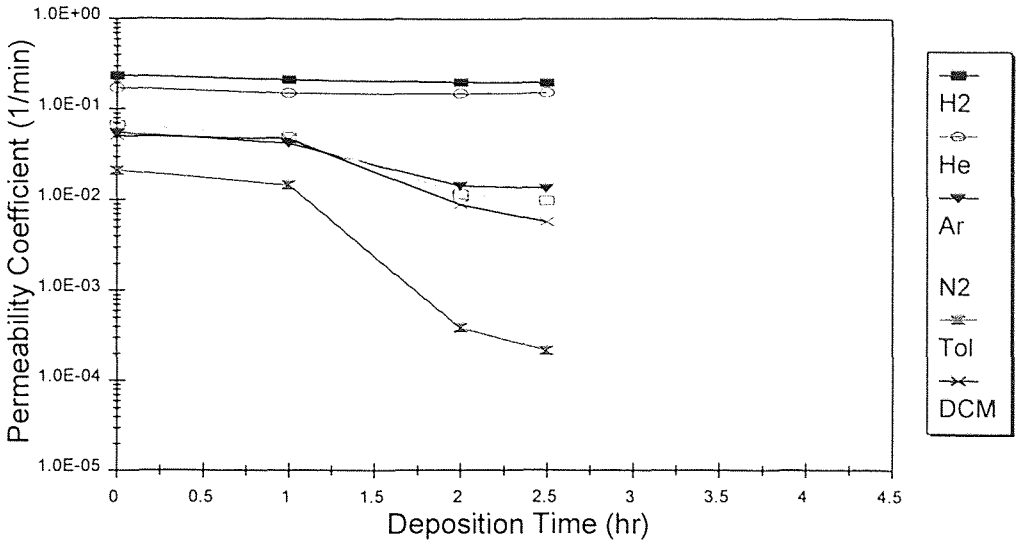

Figure 5.4: Permeabilities for Membrane III.

A noticeable drop in toluene and dichloromethane permeability was observed between depositions. This was attributed to densification of the film. Even though a deposition was not taking place, the system remained at 450°C for in-situ permeability measurements, increasing the driving force for densification. Densification was observed to have a significant effect on subsequent membranes when the pore diameter was already measured as extremely small.

Hydrogen and helium remained constant with time, while nitrogen and argon dropped, but not as significantly as toluene and dichloromethane. It was observed that this drop in permeabilities with time between depositions eventually stabilized.

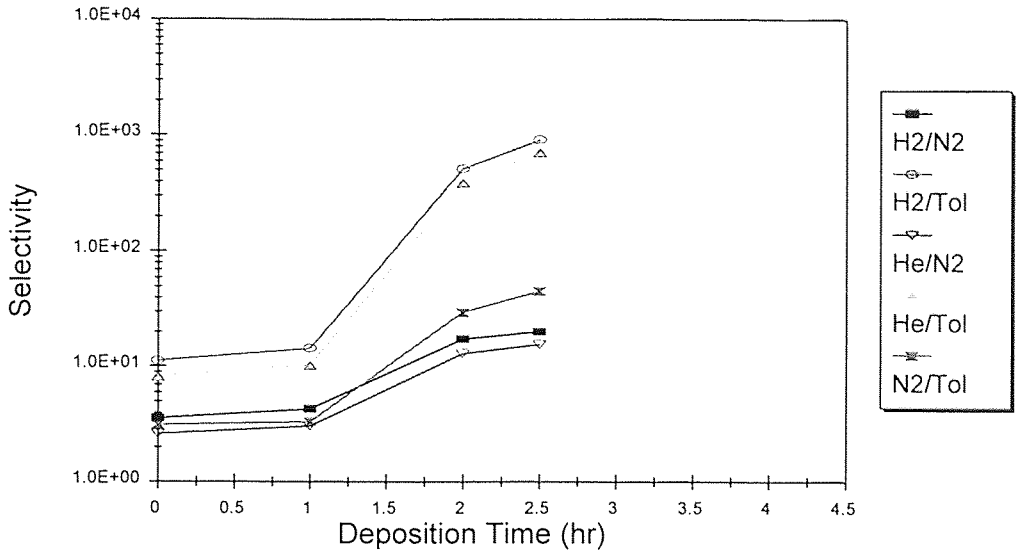

Figure 5.5: Selectivities for Membrane III.

An on-line mass spectrometer was again utilized to confirm the passage of nitrogen and/or toluene through the membrane. The first analysis of toluene with the mass spectrometer saw very small amounts of toluene passing through the membrane at each input pressure, less than 1% of the total amount of toluene introduced on the outside of the membrane had permeated through, according to the mass spectrometer. At this point in time the turbomolecular

pump on the mass spectrometer failed and rendered the analysis by this technique on subsequent tubes useless because of the unavailability of another mass spectrometer. A clear mass spectrometer analysis does not exist for Membrane III either. The mass spectrometer would not become available again until the analysis on Membrane VI.

To account for the loss of the mass spectrometer, extended permeability measurements were performed for the permeant gases, specifically nitrogen and toluene. Here, a fixed amount of permeant gas (i.e. 10 torr) was introduced into the reactor chamber and allowed to permeate through the membrane over a significant amount of time, 5 hours for example. Then plots of pressure vs. time for each gas were obtained. The graphs were typically curved as observed in Figures 5.6 and 5.7. To get selectivities, the slope of the linear portion of each graph was obtained and the ratio of N_2/toluene taken. By this method, the selectivity of N_2/toluene was 20, which was half of the value when done by the typical permeability measurements of this study. To perhaps normalize the data and obtain clearer selectivities, the pressure versus time data was plotted as $\ln[(P_o)/(P_o-P)]$ versus time where P was the pressure observed with time during the permeation and P_o was the input pressure which was constant (i.e. 10 torr). This yielded a straight line and the slope of it was taken again as the permeability. This gave a N_2/toluene selectivity value that was almost twice the previously reported N_2/toluene selectivity (70 and 45 respectively).

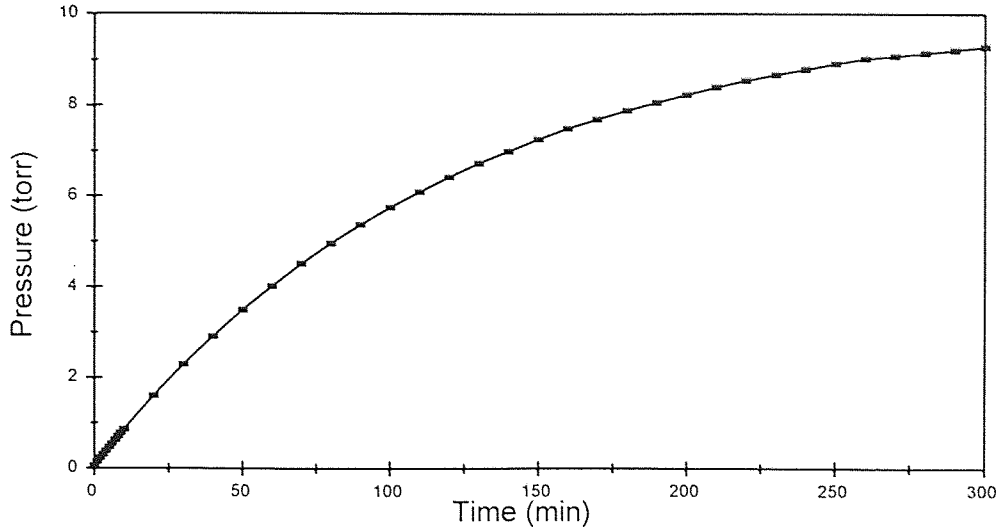

Figure 5.6: Pressure vs. Time for N_2 at 10 torr input pressure.

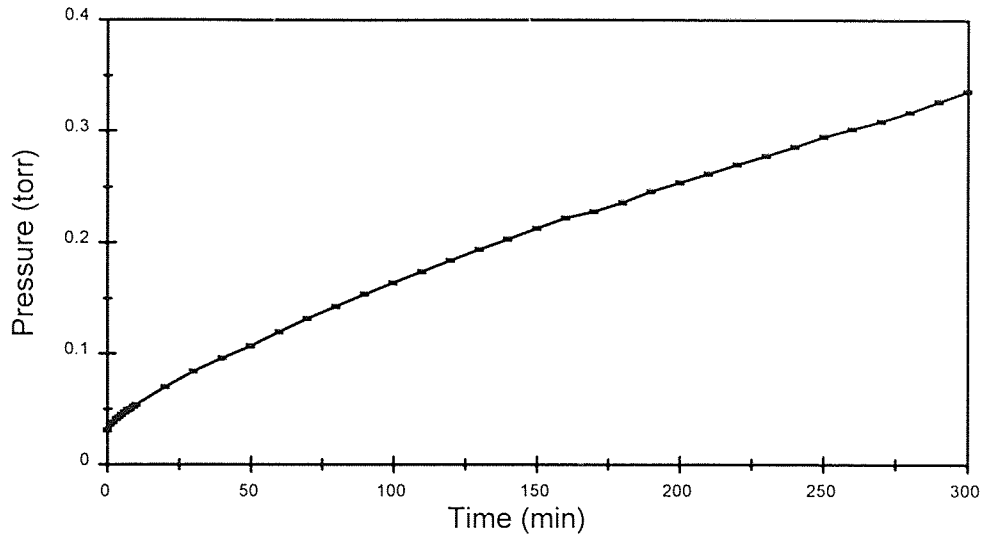

Figure 5.7: Pressure vs. Time for toluene at 10 torr input pressure.

To show how inconclusive this technique really was it was observed that the Pressure versus Time curve changed significantly with each subsequent data acquisition, decreasing the value of N_2/toluene selectivity with it. This method was not employed on subsequent membranes, staying with the dP/dt versus Pressure Difference technique which was consistently used on each membrane in this study.

5.2.4 Membrane IV

For the first hour of deposition on Membrane IV the flow rates remained at 30 sccm for DES and 200 sccm for N_2O. However, the pressure of DES inside the Vycor tube again fluctuated between 4.5 and 4.8 torr while the pressure of N_2O outside the tube remained constant at 4.5 torr. The mass flow controller was checked to see if it was calibrated correctly and it was. However, the problem persisted during the second deposition of one-half hour: the DES was stable at 4 torr, but once N_2O was introduced it fluctuated between 4.6 and 4.8 torr while the N_2O was constant at 4.5 torr. To try to stabilize the DES flow into the Vycor tube, the flow rate was reduced to 23.5 sccm for the third deposition of one-half hour which yielded a stable 4 torr DES. This was also the case for the fourth deposition of one-half hour, where DES pressure inside the Vycor tube fluctuated between 4.1 and 4.3 torr. Deeming the flow stable again, the DES flow rate was slightly raised to 27.5 sccm for the final deposition of one-half hour

to see if it would again have an adverse effect on the DES pressure. It did not as DES fluctuated only slightly between 4 and 4.1 torr during the deposition.

Permeability data for Membrane IV is given in Figure 5.8. A severe drop in the permeabilities of N_2 and Ar was seen after 2.5 hours of deposition. This decrease was much more pronounced than in the previous membranes. Toluene and DCM also drop by several orders of magnitude, but that was consistent with the permeabilities for other membranes as well. The permeability values for N_2, Ar, toluene, and DCM scale with the outgassing rate of the system.

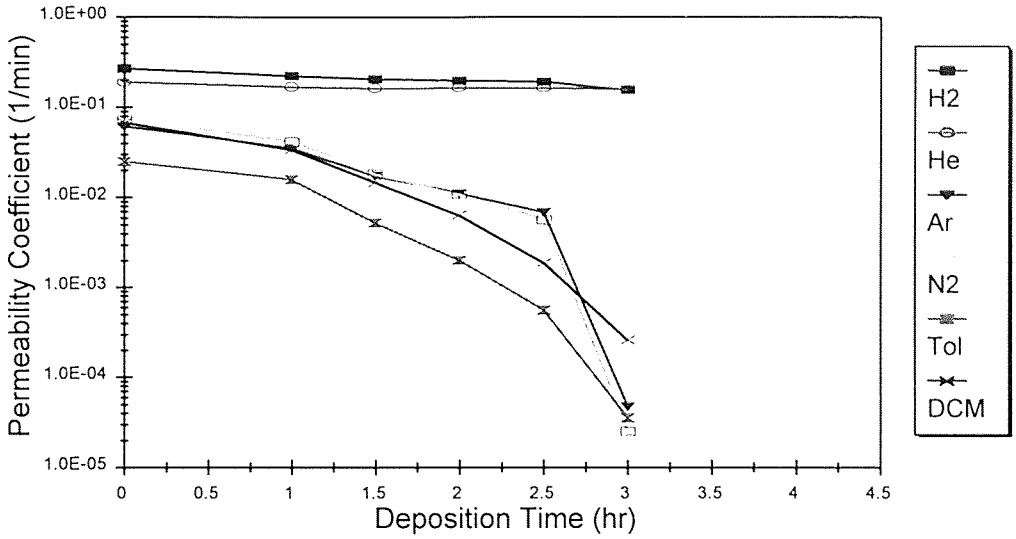

Figure 5.8: Permeability data for Membrane IV.

As the huge decrease in permeability for the VOC's was desired, the huge decrease for the inerts, especially nitrogen, was not. This suggests that this

process may not be self-limiting in the context of this study. Other factors may combine to effectively clog the pores and not allow nitrogen to pass. In this instance, the clogging mechanism could be directly attributable to the DES pressure fluctuation in the Vycor tube. The excess DES may continue to react in the pores over time especially at 450°C and in the presence of the permeant gases. The effect of pore clogging on selectivity is seen in Figure 5.9. The severe drop in permeability for nitrogen, argon, toluene, and dichloromethane produced huge selectivity values for H_2/N_2, H_2/toluene, He/N_2, and He/toluene, while severely decreasing all others. Although the pores did clog, a significant result was obtained from Membrane IV. It was observed that, although a maximum deposition time for optimal selectivity values may exist given the deposition parameters of this study, a minimum deposition time also exists where any significant selectivity over Knudsen occurs.

5.2.5 Membrane V

To maintain a steady pressure of 4 torr DES inside the tube, the flow rate was kept at 23.5 sccm for the first deposition of one hour. This was also true of the second deposition of one hour, but the DES pressure fluctuated between 4.2 and 4.3 torr. For the third deposition of one-half hour, the DES flow rate was still 23.5 sccm over the first ten minutes and the pressure remained at around 4.2 to 4.3 torr. To see if the pressure would indeed rise and fluctuate with an increase in flow rate, the DES flow was increased to the original condition of 30 sccm.

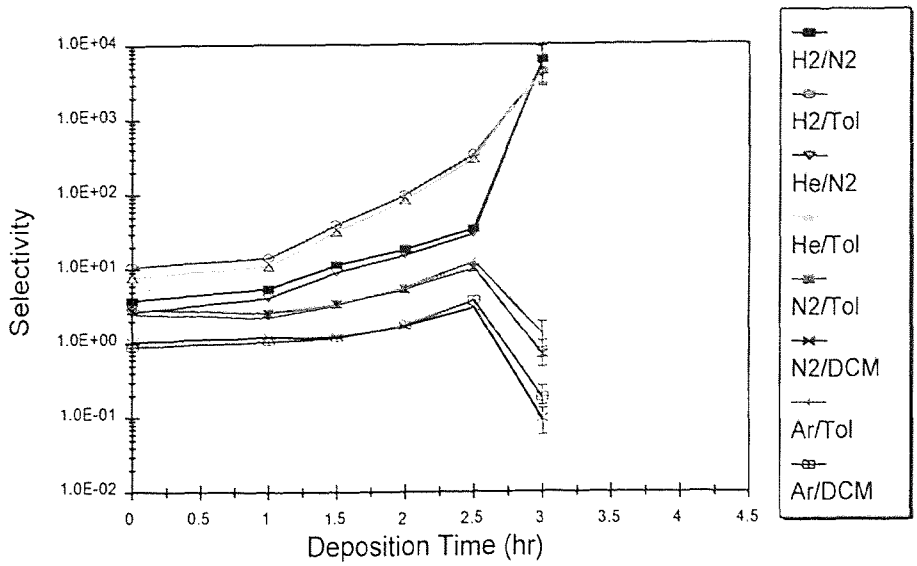

Figure 5.9: Selectivity data for Membrane IV.

When this was done, the DES pressure inside the tube rose to 4.7 torr and fluctuated between 4.5 and 4.7 torr on all subsequent depositions. N_2O pressure was steady at 4.5 torr and 200 sccm. For consistency and for direct comparison with the data obtained by Levy[28] et al and the previous data of this study, the DES flow rate was left at 30 sccm for the rest of the experiments. This was done at the possible cost of excess precursor gas during deposition and maybe pore clogging. The permeabilities did not drop as severely as in Membrane IV as seen in Figure 5.10.

Referring to the selectivities in Figure 5.11 a minimum deposition time was again observed before any significant selectivity over Knudsen occurred. Over the entire range of deposition times, H_2/N_2, H_2/toluene, He/N_2, and He/toluene

selectivity increased, as was expected and the results scale with those of previous membranes. However, after a certain deposition time, in this case 3.25 to 3.5 hours, the other selectivities, after steadily increasing, began to drop. This was evidence that an optimal deposition time may exist and the process may not truly be self-limiting. The temperature of 450°C that the reactor was kept at combined with the presence of the permeant gases may be altering the self-limiting nature of the process.

5.2.6 Membrane VI

For this membrane, the initial deposition was done over 2.5 hours because of the observed increase of selectivity after a certain deposition time. For this deposition, the DES pressure in the Vycor tube was stable at 4 torr. Permeability decreased steadily with time for all gases, as shown in Figure 5.12, except for H_2 and He, which again changed insignificantly. Although all selectivities increased over Knudsen after the first deposition, N_2/toluene and Ar/toluene went down, as seen in Figure 5.13. After the second deposition of one-half hour where the DES pressure fluctuated between 4 and 4.4 torr, these two selectivities went up, but N_2/toluene remained lower than Knudsen. After the third deposition of one-half hour where the DES pressure remained constant at 4 torr (N_2O pressure remained steady at 4.4 torr for each deposition) all selectivities began to rise except N_2/DCM, which decreased.

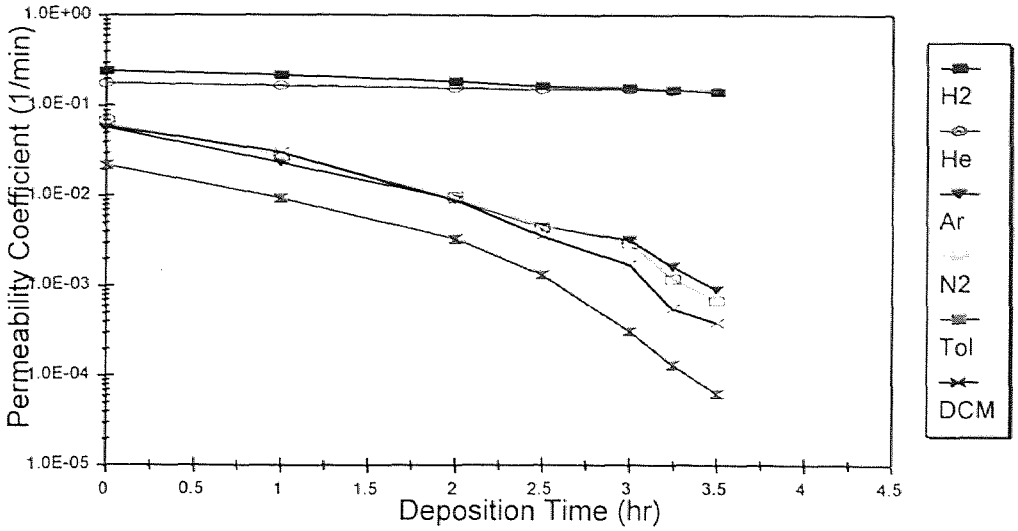

Figure 5.10: Permeability data for Membrane V.

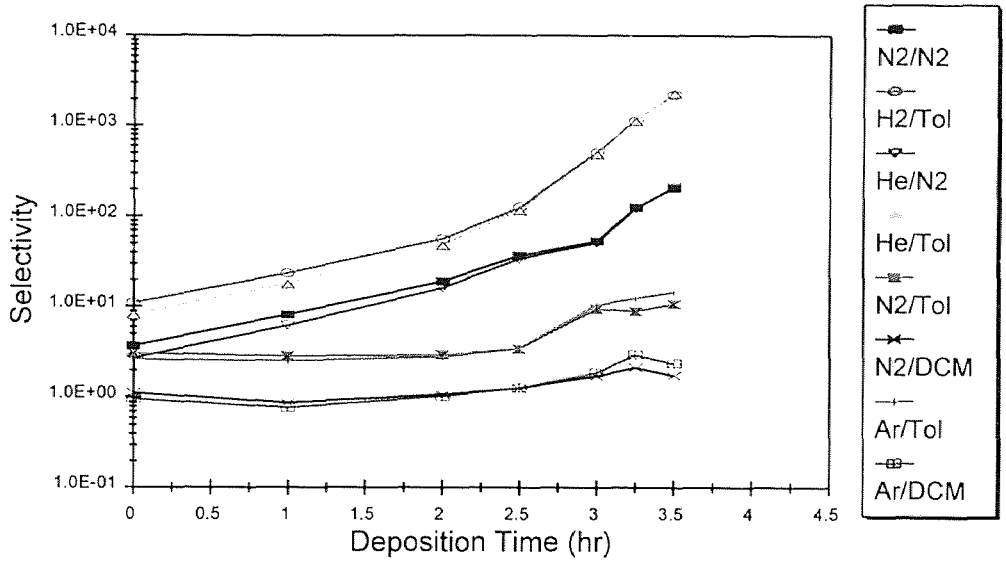

Figure 5.11: Selectivity data for Membrane V.

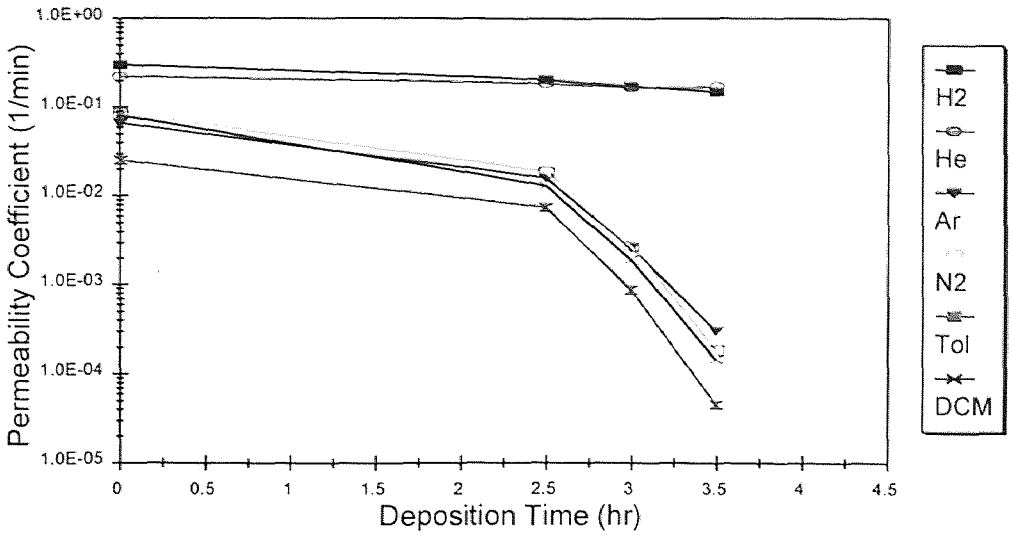

Figure 5.12: Permeabilities for Membrane VI.

The high selectivities for H_2/N_2, H_2/toluene, He/N_2, and He/toluene were directly attributed to the decrease in nitrogen and toluene permeability. Mass spectroscopy confirmed the absence of N_2 and toluene after permeability measurements. The fairly low selectivities of the other gas combinations were again the result of the low permeabilities of nitrogen, argon, toluene, and DCM. No further depositions were done on this membrane because of the very low permeability values for argon and nitrogen. After 45 days at 450°C and no subsequent depositions, the permeability of nitrogen and toluene scaled with the outgassing rate of the system, indicating that the membrane was clogged to both of them, further evidence that this process is not self-limiting. This phenomenon shows how the film characteristics depend on temperature. In-situ permeability

measurements were done on all membranes following successive depositions. In each case, the film was kept at the deposition temperature of 450°C while permeability data was collected, as per previous studies where it was found that this temperature provided the best film characteristics in the optimal amount of deposition time[28,65]. This caused the film to *densify* with time even after the deposition took place, as was evidenced by the decrease in permeability with time between depositions. In some cases, film densification was not very pronounced. But as the pores in the membrane became narrower and narrower with each successive deposition, film densification became much more of a factor in film performance, decreasing N_2 and Ar permeability significantly. To remedy this, permeability measurements should be done at a lower temperature. Although very time consuming, it would give a clearer picture as to the effect of temperature on film densification. In addition, the pore size distribution should be characterized in more detail. Several mechanisms are possible for the clogging of the membranes, one being that the film deposition is clogging the smaller pores initially and eventually reducing the larger pores to a very small pore diameter. This would explain low flow rates. Perhaps membrane structure characterization using analytical microscopy would help clarify this. It would also show if the film was depositing uniformly in the pores or if it is also depositing on the surface of the tube, which would also clog the pores.

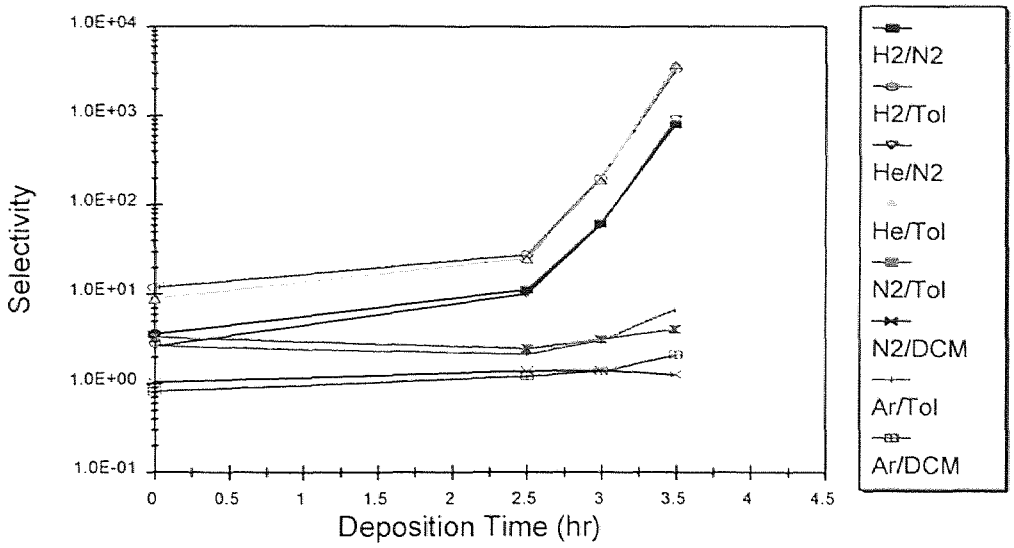

Figure 5.13: Selectivities for Membrane VI.

CHAPTER 6

CONCLUSIONS

- The pore narrowing rate, monitored in terms of decrease in gas permeabilities and increase in selectivities, increased with successive depositions, as expected. High selectivities were obtained for H_2 and He over Ar, N_2, and VOC's. In selected cases, selectivities for N_2 and Ar over VOC's, specifically N_2 over toluene, were obtained.
- The main obstacle in obtaining consistent results for inert/VOC separation was severe fluctuations in process parameters, specifically DES gas flow. This was more of a direct result of the equipment involved than the technology proposed. However, the data obtained proves these structures to be useful in separating hydrogen and helium from gas mixtures and inerts from VOC's. More work needs to be done on separating species close in kinetic diameter from each other.
- It was experimentally observed that the SiO_2 film deposition process may not be self-limiting as defined in this paper. At high deposition times, nitrogen flow was so low that it scaled with the outgassing rate of the reactor system. Film densification subsequent to deposition may be the primary cause of this phenomenon.

REFERENCES

1. C. Chiu, *Hydrocarbon Processing*, **69**, 69 (1990).

2. R. Spillman, *Chem. Eng. Prog.*, **85**, 41 (1989).

3. R. Renko, *Pollut. Eng.*, **26**, 62 (1994).

4. G. Fagliano, M. Berry, F. Bove, and T. Burke, *Public Works*, **122**, 96 (1991).

5. K.K. Chan and A.M. Brownstein, *Ceram. Bull.*, **70**, 703 (1991).

6. J. Fried, *Polymer Science and Technology*, Prentice-Hali, Englewood Cliffs, New Jersey (1995), ch.12.

7. R.E. Kesting, *Synthetic Polymer Membranes: A Structural Perspective*, John Wiley and Sons, New York (1985), p. 10.

8. H.P. Hsieh, P.K.T. Liu, and T.R. Dillman, *Polymer Jour.*, **23**, 407 (1991).

9. K. Keizer and H Verweij, *Chemtech*, **January 1996**, 37.

10. S. Hwang and K. Kammermeyer, *Techniques of Chemistry, Vol. 7*, John Wiley and Sons, New York (1975), p.57.

11. D.W. Shaefer, *MRS Bull.*, **19**, 14 (1994).

12. R.E. Cunningham and R.J.J. Williams, *Diffusion in Gases and Porous Solids*, Plenum Press, New York (1980), p.12.

13. R.A. Ulhorn and A.J. Burggraaf, in:*Inorganic Membranes*, ed. R. Bhave, Chapman and Hall, New York (1991), p. 167.

14. A.B. Shelekhin, A.G. Dixon, and Y.H. Ma, *AIChE Jour.*, **41**, 58 (1995).

15. R. Zanetti, *Chem. Eng.*, **June 9, 1996**, 19.

16. J. Haggin, *C&EN*, **June 6, 1988**, 7.

17. J.C.S. Wu and P.K.T. Liu, *Ind. Eng. Chem. Res.*, **31**, 322 (1992).

18. A.L.Y. Tonkovich, R.B. Secker, and J.L. Cox, *Sepn. Sci. and Tech.*, **30**, 1609 (1995).

19. M.V. Volf, *Technical Glasses*, Sir Isaac Pitman and Sons (1961), p.178.

20. B. Gelernt, *Semicond. Int.*, **13**, 82 (1990).

21. A.K. Hochberg and D.L. O'Meara, *J. Electrochem. Soc.*,**136**, 1843 (1989).

22. G.S. Chakravarthy, R.A. Levy, J.M. Grow, and W.M. Attia, in: *The Physics and Chemistry of SiO_2 and the Si-SiO_2 Interface* 2, ed. C. R. Helms and B. E. Deal, Plenum Press, New York (1993), p. 165.

23. G.R. Gavalas, C.E. Megiris, and S.W. Nam, *Chem. Eng. Sci.*, **44**, 1829 (1989).

24. S.W. Nam and G.R. Gavalas, *AIChE Symp. Ser.*, **268**, 68 (1989).

25. M. Tsapatsis, S. Kim, S.W. Nam, and G.R. Gavalas, *Ind. Eng. Chem. Res.*, **30**, 2152 (1991).

26. M. Tsapatsis and G.R. Gavalas, *AIChE Jour.*, **38**, 847 (1992).

27. C.E. Megiris and J.H.E. Glezer, *Ind. Eng. Chem. Res.*, **31**, 1293 (1991).

28. R.A. Levy, E.S. Ramos, L.N. Krasnoperov, A. Datta, and J.M. Grow, *J. Mater. Res.*, **11**, 3164 (1996).

29. A.J. Burggraaf and K. Keizer, in:*Inorganic Membranes*, ed. R. Bhave, Chapman and Hall, New York (1991), p. 21.

30. Q. Xu and M.A. Anderson, *J. Mater. Res.*, **6**, 1073 (1991).

31. E.T. Webster and C.G. Hill, *Sepn. Sci. and Tech.*, **30**, 1689 (1995).

32. M. Trocha and W.J. Koros, *J. Membr. Sci.*, **95**, 259 (1994).

33. A.J. Burggraaf and K. Keizer, in: *Inorganic Membranes*, ed. R. Bhave, Chapman and Hall, New York (1991), p. 23.

34. H.P. Hsieh, *AIChE Symp. Ser.*, **84**, 1 (1988).

35. J.J. Hammel, *J. Chem. Phys.*, **46**, 2234 (1967).

36. A.J. Burggraaf and K. Keizer, in: *Inorganic Membranes*, ed. R. Bhave, Chapman and Hall, New York (1991), p. 18.

37. V.M. Gryzanov, *Platinum Met. Rev.*, **30**, 68 (1986).

38. L.H. Lee and S.T. Hwang, *Chem. Eng. Comm.*, **44**, 121 (1986).

39. J.E. Koresh and A. Sofer, *Sepn. Sci. and Tech.*, **22**, 273 (1987).

40. M. Ohring, *The Materials Science of Thin Films*, Academic Press Ltd., London (1992), p. 79.

41. Y.S. Lin and A.J. Burggraaf, *AIChE Jour.*, **38**, 445 (1992).

42. K.F. Jensen, in: *Chemical Vapor Deposition*, eds. M.L. Hitchman and K.F. Jensen, Academic Press, Ltd., London (1993) p.31.

43. R.S. Rosler, *Solid State Tech.*, **20**, 63 (1977).

44. A.C. Adams, in: *VLSI Technology*, ed. S.M. Sze, McGraw-Hill, Princeton, New Jersey (1983), ch. 3.

45. R.C. Rossi, in: *Handbook of Thin-Film Deposition Processes and Techniques*, ed. K.K. Schnegraf, Noyes Publications, Park Ridge, New Jersey (1988), ch.3.

46. S. Middleman and A.J. Yeckel, *J. Electrochem. Soc.*, **133**, 1951 (1986).

47. C.R. Kleijn, T.H. van der Meer, and C.J. Hoogendoorn, *J. Electrochem. Soc.*, **136**, 3423 (1989).

48. D.M. Smith, D.W. Hua, and W.L. Earl, *MRS Bull.*, **April 1994**, 24.

49. A. Bottino, G. Capannelli, and P. Petit-Bon, *Sepn. Sci. and Tech.*, **26**, 1315 (1991).

50. H.P. Hsieh, in: *Inorganic Membranes*, ed. R. Bhave, Chapman and Hall, New York (1991), p. 74.

51. J. Rocek and P. Uchytil, *J. Membr. Sci.*, **89**, 119 (1994).

52. P. Mikulasek and P. Dolecek, *Sepn. Sci. and Tech.*, **29**, 1183 (1994).
A.E. Derome, *Modern NMR Techniques for Chemistry Research*, Pergamon Press, Oxford (1987).

53. H.P. Hsieh, in: *Inorganic Membranes*, ed. R. Bhave, Chapman and Hall, New York (1991), p. 76.

54. F.P. Cuperus, D. Bargeman, and C.A. Smolders, *J. Membr. Sci.*, **71**, 57 (1992).

55. D.E. Fain, *Proc. First Intl. Conf. Inorganic Membranes*, **July 1989**, 199-205.

56. G. Cao, H.W. Brinkman, J. Meijerink, K.J. de Vries, and A.J. Burggraaf, *J. Am. Ceram. Soc.*, **76**, 2201 (1993).

57. A. Mey-Marom and M. Katz, *J. Membr. Sci.*, **27**, 119 (1986).

58. R.J.R. Ulhorn, K. Keizer, R.J. Vuren, and A.J. Burggraaf, *J. Membr. Sci.*, **39**, 285 (1988).

59. H.P. Hsieh, in: *Inorganic Membranes*, ed. R. Bhave, Chapman and Hall, New York (1991), p. 80.

60. R.J.R. Ulhorn and A.J. Burggraaf, in: *Inorganic Membranes*, ed. R. Bhave, Chapman and Hall, New York (1991), p. 156.

61. J.C.S. Wu, D.F. Flowers, and P.K.T. Liu, *J. Membr. Sci.*, **77**, 85 (1993).

62. J.D. Way and D.L. Roberts, *Sepn. Sci. and Tech.*, **27**, 29 (1992).

63. R.J.R. Ulhorn and A.J. Burggraaf, in: *Inorganic Membranes*, ed. R. Bhave, Chapman and Hall, New York (1991), ch. 6.

64. M. Asaeda and L.D. Lu, *J. Chem. Eng. Japan.*, **19**, 72 (1986).

65. C. Ravindranath, M.S. Thesis, Interdisciplinary Program in Materials Science and Engineering, New Jersey Institute of Technology, Newark, New Jersey, October 1995.